Understanding the role of solvent in determining the size and catalytic behaviour of Pd Nanocrystals

Parmeet Kaur Dhindsa

A dissertation submitted for partial fulfilment of
BS-MS dual degree in Science

Indian Institute of Science Education and Research Mohali
June 2020

Certificate of Examination

This is to certify that the dissertation titled "**Understanding the role of solvent in determining the size and catalytic behaviour of Pd nanocrystals**" submitted by **Ms. Parmeet Kaur Dhindsa** (Reg. No. MS15017) for the partial fulfilment of BS-MS dual degree programme of the Institute, has been examined by the thesis committee duly appointed by the Institute. The committee finds the work done by the candidate satisfactory and recommends that the report be accepted.

Dr. Debrina Jana Dr. A. R. Choudhary Dr. Ujjal K Gautam
(Supervisor)

Dated: June 2020

Declaration

The work presented in this dissertation has been carried out by me under the guidance of Dr. Ujjal K. Gautam at the Indian Institute of Science Education and Research Mohali. This work has not been submitted in part or in full for a degree, a diploma, or a fellowship to any other university or institute. Whenever contributions of others are involved, every effort is made to indicate this clearly, with due acknowledgement of collaborative research and discussions. This thesis is a bonafide record of original work done by me and all sources listed within have been detailed in the bibliography.

Parmeet Kaur Dhindsa
MS15017

Dated: June 2020

In my capacity as the supervisor of the candidate's project work, I certify that the above statements by the candidate are true to the best of my knowledge.

Dr. Ujjal K Gautam
(Supervisor)

Acknowledgement

With great pleasure and reverence, I express my deep sense of gratitude, respect and obligation to my project supervisor Dr. Ujjal K Gautam (Department of Chemical Sciences, IISER Mohali) for his constant support, encouragement, fruitful discussions and invaluable suggestions. His enthusiasm in research have always been guiding light for me throughout my research project and played a vital role in moulding myself as an innovative researcher. I thank him for developing scientific research aptitude into me, starting from thinking critically to writing scientific manuscript.

I express my sincere thanks to Prof. J. Gowrishankar (Director, IISER Mohali) and Prof. S. Arulananda Babu (Head of Dept. Of Chemical Sciences, IISER Mohali) for providing excellent infrastructural facilities. I wish to thank staff associated with IISER Mohali, especially TEM facility for their assistance and help. I would also like to thank my committee members Dr. A. R. Choudhary and Dr. Debrina Jana.

I am thankful to Lipipuspa for her wholehearted support and supervision. My heartfelt thanks are due to my lab mates Sanjit, Sandita, Nihal, Reeya, Maqsuma , Raj , Komal for their cooperation and friendly atmosphere in the lab. Finally, I would like to acknowledge my classmates and friends for my memorable time at IISER Mohali.

Parmeet Kaur Dhindsa

List of Figures

List of Tables

List of Abbreviations

EIS	electrochemical impedance spectroscopy
EG	Ethylene glycol
k	rate constant
M	molarity
nm	nanometre
NMR	nuclear magnetic resonance
NC	nano catalysts
PVP	polyvinylpyrrolidone
rpm	revolutions per minute
s-TOF	Surface turn over frequency
TEM	transmission electron microscopy
UV	ultraviolet
VIS	visible
V_{oc}	open circuit potential
%(v/v)	% volume fraction
XRD	x-ray diffraction

Table of Contents

Abstract

Solvents of synthesis can influence not only the size and shape of nanoparticles but also their catalytic properties. In an effort to understand the effect of solvents during the solvothermal synthesis of Pd nanocrystals (NCs), and the consequent effect in their catalytic properties, nearly monodispersed quasi-spherical nanoparticles have been synthesized by reduction of metal precursor salt H_2PdCl_4 using polyvinylpyrrolidone (PVP) as both reducing and capping agent in the solvent mixtures of water and ethylene glycol (H_2O-EG) in varying composition. Various characterization techniques such as transmission electron microscopy (TEM), powder X-ray diffraction (PXRD), Fourier transform infrared (FTIR) spectroscopy were utilized to explicate how methodical increase in the fraction of EG : 0%(v/v), 25%(v/v), 50%(v/v), 75% (v/v), 100%(v/v) in the mixture of H_2O-EG govern Pd NCs size and thus catalytically active surface area. The progression of Pd NCs size with an increasing fraction of EG shows a correspondence between the viscosity, boiling point, and dielectric constant of solvent and NCs size. This is also explained using Hansen solubility parameters which predicts solvent-mediated stability of capping agent around Pd nuclei during the growth step. Secondly, to gain insight into the influence of solvent used on Pd NCs catalytic activity, the above synthesized different sized Pd NCs efficiency is compared by carrying out Suzuki- Miyaura cross-coupling reaction and catalytic nitro-aromatic reduction reactions. A substantial difference observed in surface normalized turn over frequencies (TOF) and kinetic rate constants accentuate a deeper role of solvent beyond size control of NCs. This disparity in surface area normalized catalytic efficiencies is attributed to solvent-caused subtle differences in the surface energy due to factors such as different coverage density of capping agent PVP around Pd NCs, and the nature of surface atoms.

1. Introduction

When size scale is down to nanoscale (1-100 nm), unique chemical and physical properties emerge out of metal, oxides and semiconductors.[1] These nanoarchitectures, in turn, have found their applications in many emerging fields such as catalysis for organic reactions, sensing, plasmonics and electrocatalysis. It is well established that these properties and promising applications are not only related to their intrinsic matter themselves but also their existing form and morphology. Mastery over the size, shape, structure, crystallinity, composition and surface chemistry of a nanocrystal enables control of its properties and enhancement of its usefulness for a given application (Figure1).[2] In the field of catalysis, the size and morphology of the nanoparticles (NP, the quantum confinement effect as well as the proportion of atom at corners, edges and faces) essentially modulate their catalytic performance.[3,4] The presence of a high density of low-coordinated atoms is beneficial for enhancing the number of active sites.[3] In general, high-index facets have exhibited higher catalytic activities than low-index ones. Nanoparticles may also have cavities on the surface that would affect specific surface-active area available for catalytic reactions.[5] The surface charge is as equally important as size or shape. Nanoparticles are often capped with polymers and other ligands that can affect adhesion to surfaces and agglomeration characteristics owing to the different surface charges.[6] In the view of the highly dependent catalytic activity on the nano-construction, there has been a tremendous surge in research activity related to the synthesis and characterization of metal nanocrystals with homogenous size and shape.[7]

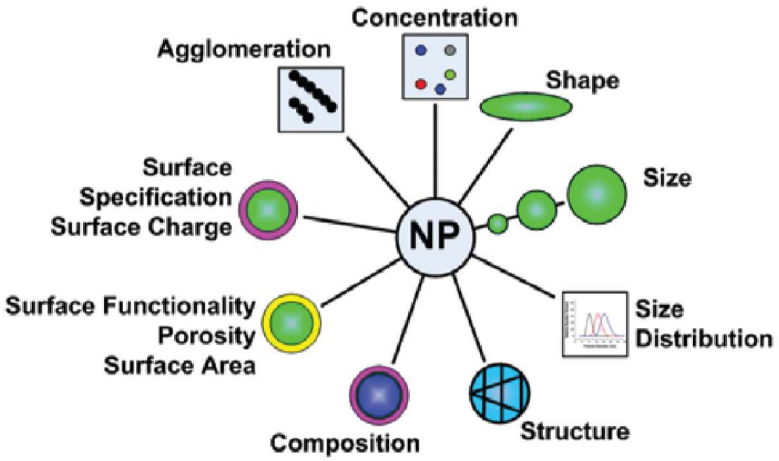

Figure 1. Key parameters to characterize nanomaterials.[6]

Much of the current research has been devoted to engineering structural morphologies such as by varying metal precursors, solvents, reducing agents, synthesis routes, reaction conditions (temperature, pressure, and pH) and use of organic surface grafting agents like polyvinylpyrrolidone (PVP).[8–17] Traditionally, progress in this area has taken place by an observation-driven and hit and trial approach. To head towards a design-driven era in the synthesis of metal nanoparticles, it is central to understand the fundamental steps involved in the synthesis. In a typical synthesis, for example, the formation of metal nanocrystals can be divided into three stages: (i) nucleation from the atoms formed by reduction of metal salts, (ii) evolution of nuclei into seeds, and (iii) growth of seeds into nanocrystals through a process of atomic addition. By altering the experimental parameters, nucleation and growth rates are usually manipulated, providing the means for controlling the size and shape of the nanocatalysts. Fast nucleation results in a high nuclei concentration and yields small particles, while a slow nucleation results in a low concentration of nuclei and results in a population of proportionally larger particles (Figure 2).[18] The acquisition of NPs with desired characteristics requires a reasonable understanding of the role played by each of the parameters.

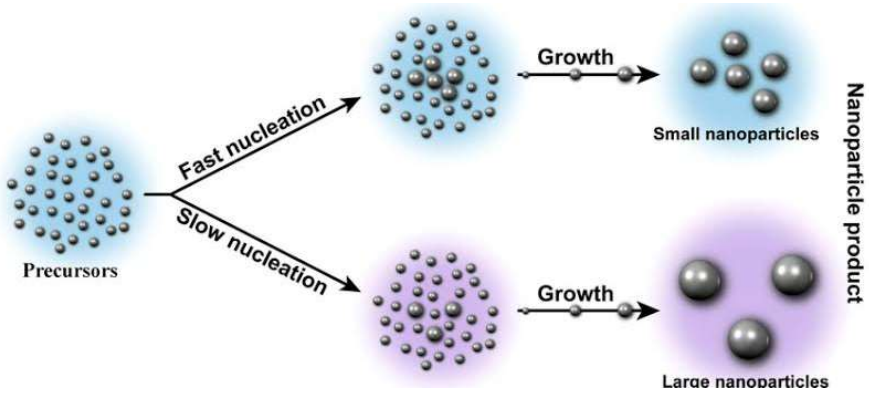

Figure 2. The brief formation mechanism of metal nanoparticles.[18]

1.1 Role of solvent in synthesis of the desired nanocatalysts

There exist many reports where the solvent used during synthesis is the crucial factor for tuning of the size and shape of the nano catalyst.[19–35] Being the medium of the reaction, the solvent can play a significant role in controlling the reaction dynamics and kinetics. Douglas group had explored the relevance of viscosity and boiling point of the solvent in solvothermal synthesis of magnetite NPs.[36] They found an increase in particle size consistent with the increase in solvent viscosity. Here, greater viscosity of the solvent is seen to limit species mobility and hence favoured slow nucleation of NP nuclei. This left more precursor in the solution for subsequent growth and thus larger size NPs were

obtained. Likewise, Jiang et. al observed larger gold nanoparticles and with more tips on increasing the viscosity of the reaction solvent (Figure 3).[30] The boiling point of the solvent sets the maximum attainable temperature or pressure, which determines the rate of decomposition of the metal precursor. For solvents with lower boiling points and consecutively the higher saturated vapor pressure, the growth of nuclei gets limited.

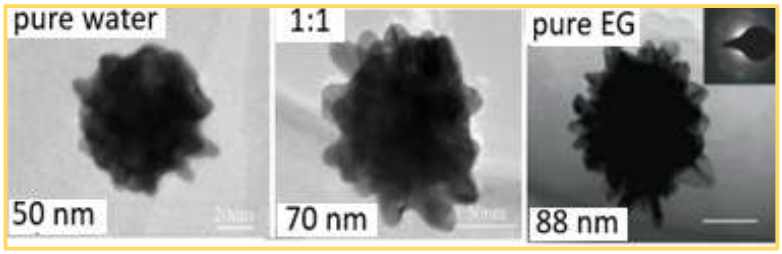

Figure 3. Gold nanoflowers synthesized in mixtures of water and EG.[30]

The polarity, dipole moment and dielectric constant of the solvent also change the reactivity of reducing agents and precursors and stability of nuclei.[28] For instance, Song and his group had controlled the size of AuNPs by varying the composition of benzene: $CHCl_3$ solvent mixture during synthesis (Figure 4). The decrease in particle size in a higher fraction of $CHCl_3$ was attributed to the limited stability of larger particles in the polar solvent (i.e., higher fraction of $CHCl_3$) because of their strong van der Waals attraction. Likewise, particle size-controlled growth of Pt nanoparticles through varying the H_2O volume percent during their synthesis has been reported, where the presence of water accelerated the reduction pathway of metal precursor.[29]

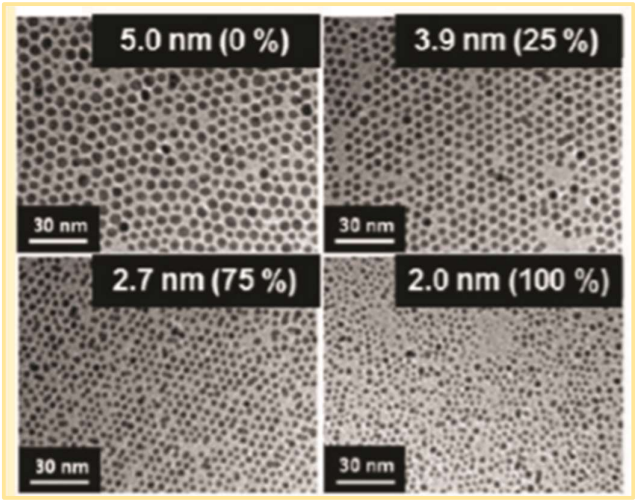

Figure 4. Solvent controlled synthesis in benzene-$CHCl_3$ solvent mixtures.[28]

Furthermore, Maharaz group found for microwave-assisted PbS nanoparticle synthesis that with increasing the dipole moment of solvents, crystallite size decreases.[21] This is because

solvents with high dielectric constant tend to stabilize ions. Xu and co-workers had shown how solvents with different polarities and saturated vapor pressures can affect the shape and morphology of ZnO samples by adjusting the solubility of the precursor in the particular solvent, initial nucleation, agglomeration and preferred orientations of the crystals,[37] In case of lower polarity solvents, owing to weaker interactions, less anisotropic growth rates were observed. Another recent work reported by the Semlali group describes a similar effect.[38] They studied the solvent effect on silicon nanoparticle (Si NP) size. The solvent apart from changing the reactivity of reducing agents and precursors, either stabilizes the nanoparticles or promotes their aggregation.

Many synthesis routes involve the use of capping agents as the surface stabilizer and growth modifier and reducing agent. These capping agents can change the order of free energies of certain facets through their interaction with the metal surface.[39] The solvent may interfere with the grafting ability of these surfactant molecules and thus influence size and shape. For example, the study by Costanzo group reveals that changing the nature of the solvent significantly impacts surfactant molecules' solvation and hence the final size of Co NPs.[20] The formation and stability of the ligand layer around NPs were influenced by the choice of the solvent used. Increasing stability of the ligand layer hindered the crystal growth process and thus smaller nanocrystals were obtained. Solvent has played an enormous role in the controlled synthesis of nanoparticles in different ways starting from affecting reducing the ability of precursor, nucleation till the growth rate of crystals. However, the influence of solvent is not considered as an important parameter as others to obtain controlled structure and morphology.

The choice of solvent used during the synthesis of NPs would also have an impact on their chemical and physical properties of the catalyst, in particular the surface properties which can tremendously influence their ability as catalysts. It becomes imperative to understand this often-overlooked impact of solvent used during nanoparticle synthesis on its catalytic activity. There are few accounts where experimental results reflect a deeper role of solvent beyond as a size constraint.[4,22,25,40–44] For instance, Xu and co-workers had reported no correlation between surface areas of ZnO NPs (synthesized in different solvents)and their respective photocatalytic activity data demonstrating that other more important factors govern activity, such as crystal habits and defects (Figure 5).[37] The crystal growth habit is known to be dependent on the interface-solvent interactions. Thongam and the group observed remarkable changes in the properties (concentration of crystal defects) of ZnO

nanostructures due to variation of the solvent of synthesis which strongly influenced their photocatalytic dye degradation ability.[43] The nanoparticles may have occlusions and cavities on the surface, which also depend on the characteristic nature of the solvents of synthesis. This would offer differential binding configuration and strength for the reacting molecules involved in a catalytic reaction by providing different sites of surface terraces, steps and corners.[5]

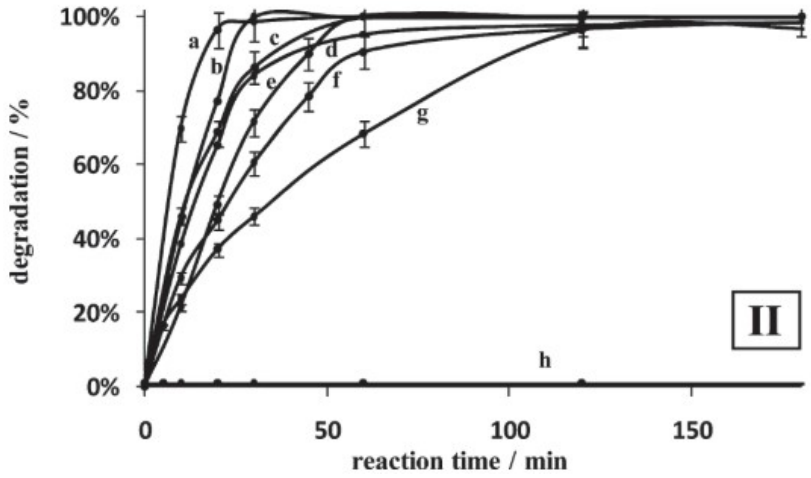

Figure 5. Performance of the catalysts for phenol photodegradation synthesized in (a) THF, (b) decane, (c) H_2O, (d) toluene, (e) ethanol, (f) acetone (g) commercial ZnO, and (h) without catalyst.[37]

Apart from modifying the growth pattern of nanocatalyst, the solvent can also alter their electronic environment. Solvents can have an affinity for certain sorts of surface atoms.[45] This can cause modification of the local electron density of the surface of the nanoparticles, depending on the nature of solvent-nanoparticle interaction. The differences in the local electronic environment could result in a large difference in activation barrier for dissociation of reactant molecules.[46] This would unanimously tailor the approach of the reacting species and thereby affect their catalytic performance. The work carried out by Luis *et. al* illustrates that strongly bound solvent molecules tend to considerably deplete the electron density of the metal surfaces.[19] They had prepared Pt NCs in different solvents and compared their catalytic activity. From XPS studies it was revealed that the outer electronic field of metal gets altered with changing the polarity of the solvent. The interaction between metal and solvent during synthesis can contribute to charge-transfer as well as of the polarization at the interface, thus altering the surface potential (Figure 6).[47]

In addition to causing geometric and electronic variations of the surface, the solvent of synthesis will also influence the coverage density of the polymer capping agent and other

cofactors e.g. ions around the nanocrystals. Although an excess of capping agents can be stripped off from nanoparticles by extensive washing, there are always residuals resistant to removal. The presence of capping agents usually restricts the free access of reactants to the surface and hence mask its catalytically active sites, atleast partially.[48] They also act as a surface modifier and improve catalytic performance.[49] The ultimate catalytic capability of these capped nanoparticles is greatly dependent on the thickness of the shell formed due to ligands.[46] The choice of the solvent of synthesis can offer control over this ligand encapsulation of the nanoparticles by modifying inter and intramolecular interaction among ligand, metal, and solvents.[20]

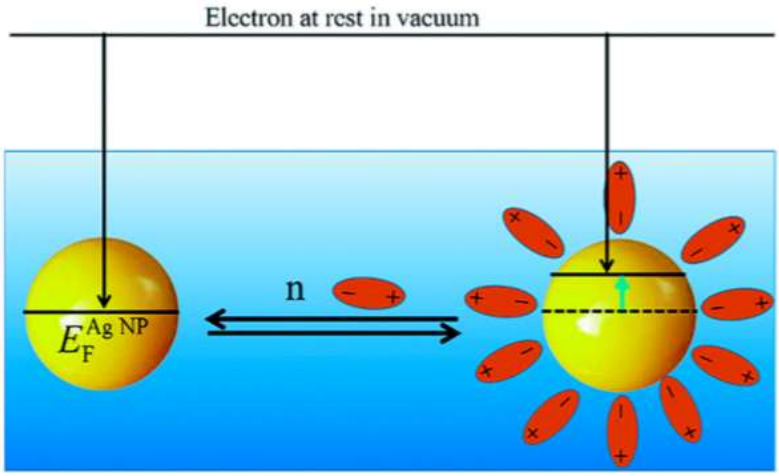

Figure 6. The relative Fermi level shift of Ag nanoparticles in the presence of a polar solvent.[47]

The solvent can also affect the orientation of the capping agent that would determine their extent of the steric hindrance. Shon et. al showed that solvent influences conformations of the ligand.[50] They observed that dodecylthiosulfate assumes alternatively outstretched or huddled conformations in non-polar or polar solvents, respectively (Figure 7). As a general assumption, the balance between the intramolecular interactions (cohesion energy) and the metal-molecule binding forces (adhesion energy) governs the molecular orientation at the metal-ligand interface. The solvent can alter the balance between these forces. When metal-ligand interactions dominate, a flat-lying arrangement is favoured, blocking the great number of active sites, whereas for prevailing intramolecular interactions, a standing up orientation is preferred.[46] This configuration allows higher catalytic activity by decreasing the fraction of poisoned sites.[51] The final geometry will be an intermediate between these two extremes, modulated through the interplay of solvent, ligand and metal interactions.

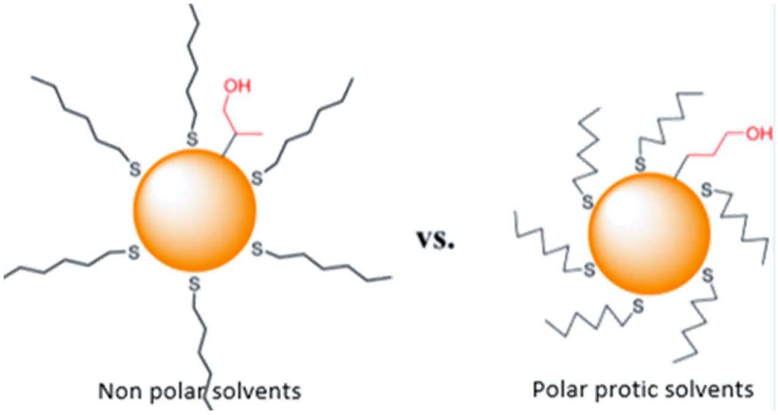

Figure 7. The effect of solvent in determining the orientation of ligand molecules.[50]

From the above discussion, it is apparent that solvents can operate not only as an experimental parameter to obtain desired nanoparticle size and shape, but also play an important role in modulating the catalyst surface. How and to what extent will the solvent of synthesis cause change in the interaction between the surface of catalyst and reactant /substrate is still an open question. Nanoparticles having similar surface area and chemical composition though expected to have similar catalytic properties can show quite dissimilar catalytic abilities. For example, McManus et. al had reported different initial rates of hydrogenation in various solvents by the same Pt/TiO_2 catalyst.[52] Hensen and others found that the surface area normalized reaction rate for silver particles in range 20 - 40 nm decreases with increasing size.[53] Likewise, Silvestre observed that TOF normalized by the total number of Pd surface atoms for butadiene hydrogenation by $Pd–Al_2O_3/NiAl$ catalysts is dependent on size (Figure 8).[54]

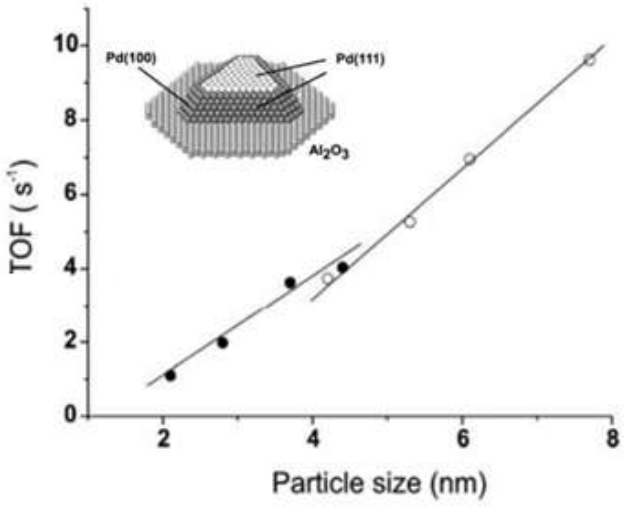

Figure 8. Turnover frequency (TOF) for the different Pd–Al2O3/NiAl normalized by the total number of Pd surface atoms for Pd(100) and Pd(111).[54]

The synthesis procedure of the nanoparticle will establish their eventual surface properties. Nanoparticles prepared in different solvents can have different surface properties and show different reactivities. If this is the case, it is important to optimize the surface for a particular reaction using a suitable solvent of synthesis. In contrast, when catalysts are used for organic transformation, it is routine to carry out screening of the solvent medium of reaction, as it can greatly enhance the catalytic activity. The same, for example, has been comprehensively reviewed by Sherwood and group where the role of solvent as the medium in chemical transformations has been illustrated with a number of literature examples.[55] Parker et al. found that the catalytic activity in the Heck reaction is susceptible to the solvent effects.[56] Figure 9 shows the correlation between the initial rate of heck coupling reaction (between iodobenzene and methyl acrylate) and the bipolarity of the solvent. The selectivity, conversion, and yield of Buchwald–Hartwig reaction is also depended on solvent polarity (Figure 10).[55]

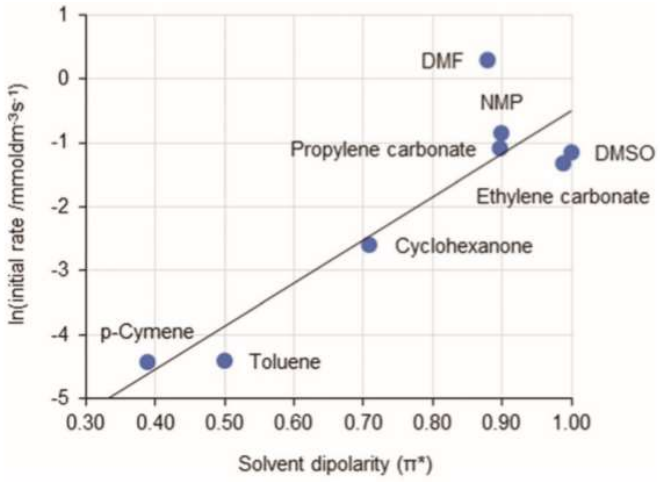

Figure 9. A linear solvation energy relationship correlating the rate of a Heck reaction with solvent polarity.[56]

Heidari et.al had investigated the effect of various media such as water, tetrahydrofuran, ethylene glycol, etc. for optimizing of Suzuki-Miyuara coupling reaction.[57] Such experimental data suggests that the solvent itself can have a direct role in activating catalysts. The solvent is the key to tuning the electronics of the catalyst and stabilizing activated complexes, ensuring the continuing of the reaction. The yields of reaction products, rate of reactions significantly depended on the solvent of reaction. To come up with the most effective conditions for the catalyst, testing of the compatibility of solvent-catalyst pairings is necessary. Similarly, it is a natural question to ask, is solvent optimization during the synthesis of nanocatalyst also a necessary step for obtaining desired

catalytic activity? As discussed earlier, the solvent of synthesis can alter the physical and chemical properties of the catalyst. It is not possible to completely get rid of stabilizers residing on the surface. This will certainly influence its ultimate reactivity. While it is normal to optimize solvents to be used during the catalytic reaction, the solvent is not known to be optimized from the synthesis point for enhancing its catalytic efficiency. It is unclear to what extent the solvent optimization during nanocatalyst synthesis can improve catalytic efficiency.

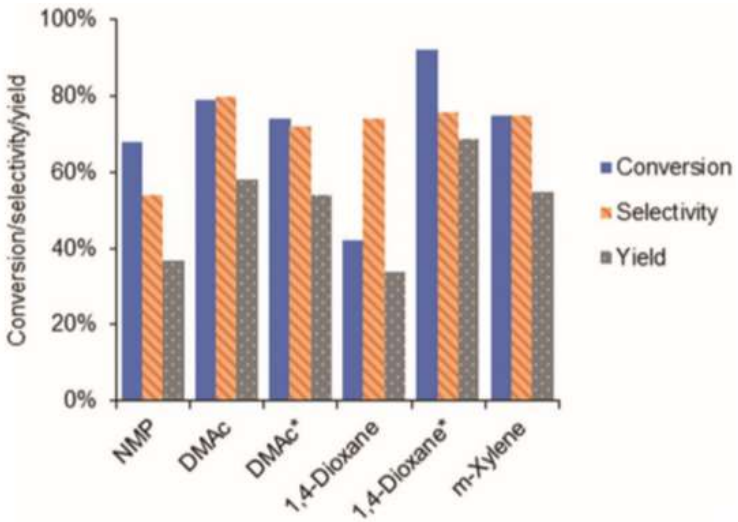

Figure 10. Comparison of the performance of a Buchwald–Hartwig reaction in different solvents.[55]

1.2 Palladium as nanocatalyst

Palladium being noble d^8 metal is catalytically very important due to its unique characteristics. Pd shows two stable oxidation states 0 and +2 and facile shuttling between the two due to relatively less activation barrier.[58] The lower activation barrier results in more rapid reactions and hence a high rate constant for the catalyst. Pd is a promising substitute for Pt in electrocatalysis as it is 50 times more abundant on earth than Pt.[59] Palladium has gained widespread use in numerous surface reactions, such as electrocatalysis (e.g. hydrogen oxidation) and coupling reactions (e.g. Heck, Sonogashira reactions). Hydrothermal synthesis is one of the various approaches that have been frequently adopted for size and shape-selective synthesis of Pd NCs.[59] Hydrothermal synthesis is not only a simple single-step process that minimizes waste, it also enables the ability to exploit the temperature and pressure-dependent properties of solvents and the selection of nontoxic reducing agents, which places the hydrothermal method among other promising "green" synthesis techniques.[59]

In the following section, two of the well-known catalytic applications of Pd, namely Suzuki Miyuara coupling and catalytic hydrogenation of nitroaromatic compounds has been briefly discussed. The EIS (Electrochemical impedance spectroscopy) technique used for characterizing the surface of the nanocatalyst has also been briefly explained.

A. Suzuki- Miyuara Coupling reaction

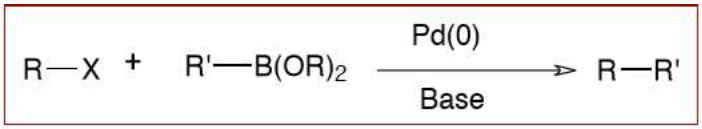

Figure 11. Suzuki C-C coupling reaction

The Suzuki Miyuara coupling reaction as represented by Figure 11 involves the cross-coupling of organohalides (and their equivalents) with organoboron reagents. The general mechanism of the Suzuki Miyuara coupling reaction using a Pd NCs is shown in the scheme in Figure 12.[60] The reaction begins with a Pd (0) catalyst. The catalyst is combined with aryl halide (Ar-X) and, through a process of oxidative addition, the palladium catalyst reacts to form Ar-Pd (II)-X complex. With the help of a suitable base, the palladium center gets activated, along with the elimination of halide ion. The base will also coordinate with boron in phenylboronic acid (Ar`-$B(OH)_2$ and makes Ar` group more nucleophilic. This enables Ar-Pd(II)-X to undergo transmetallation with phenylboronic acid (Ar`-$B(OH)_2$, to produce Ar-Pd(II)-Ar` complex. Finally, the palladium is detached from between the two aromatics via reductive elimination, producing the diaryl product (Ar-Ar`) and refreshing the palladium catalyst for another cycle.

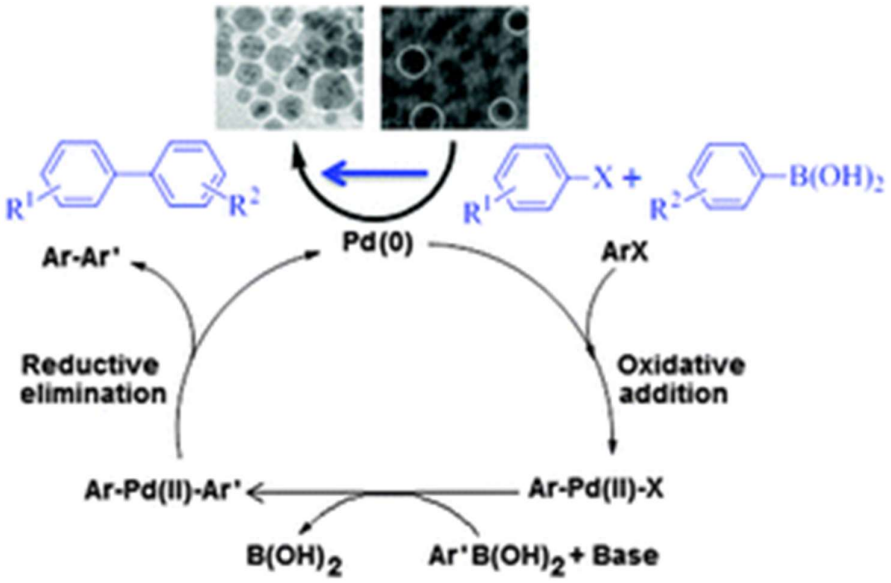

Figure 12. General mechanism of Suzuki Miyuara coupling reaction.[60]

B. Nitro-aromatic compounds reduction

Catalytic hydrogenation is an efficient method for the generation of aromatic amines from aromatic nitro compounds. Figure 13 depicts the reduction of 4-nitrophenol (4-NP) on the nanoparticle surface. The reaction involves a series of electron and proton transfers, which occurs on the nanocatalyst surface (Figure 13). The nitro group is reduced to the nitroso group, followed by the reductive addition of two hydrogen atoms to form hydroxylamine. Finally, the hydroxylamine is further reduced to the aniline derivative.

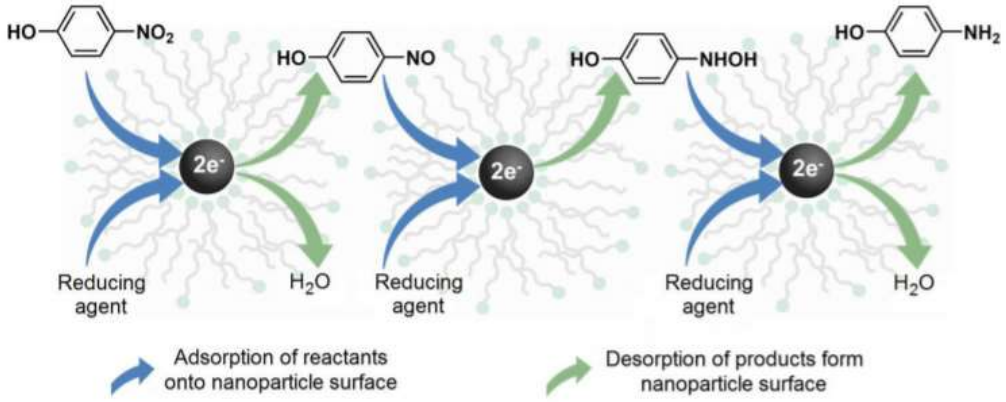

Figure 13. Reduction of 4-NP on the nanoparticle surface.[61]

Kinetic study of catalytic reduction

The kinetic equation of the reaction can be written as,

$$\frac{-\partial C_t}{\partial t} = k'[NaBH_4]^m[C_t]^n$$

where m and n are the reaction orders of [$NaBH_4$] and [4-NP] respectively. C_t is the concentration of 4-NP at time t, and k' is the rate constant. For this reaction, $NaBH_4$ is taken in excess amount and therefore this reduction reaction can be presumed to follow first-order kinetics. As $NaBH_4$ concentration is in large excess compared to 4-NP, the above equation can be simplified as,

$$\frac{-\partial C_t}{\partial t} = k\,[C_t]^n$$

$$\ln\left(\frac{-\partial C_t}{\partial t}\right) = nln([C_t]) + lnk$$

Since the reaction follows pseudo-first-order kinetics, the value of n is taken as 1. On integrating with respect to time. the equation becomes,

$$ln\left(\frac{C_t}{C_0}\right) = -kt$$

Where C_0 corresponds to the initial concentration of 4- NP and k is the apparent rate constant.

Beer-Lambert law is the linear relationship between absorbance and concentration of an absorbing species. According to this law, the absorbance of a solution can be expressed as,

$$A = \varepsilon lC$$

Where A is the measured absorbance, ε is the wavelength-dependent molar absorptivity constant, l is the path length of the sample, and C is the concentration of the analyte in solution. Since the path length has a constant value, the absorbance and concentration are directly related. Thus, the equation can be rewritten as,

$$ln\left(\frac{A_t}{A_0}\right) = -kt$$

Where A_0 is the initial absorbance of the solution at time t=0 and A_t is the absorbance of the solution at time t.

C. Electrochemical Impedance spectroscopy

Electrochemical impedance spectroscopy (EIS) can be used to characterize the bulk and interfacial properties of the system. The principle of EIS is to perturb the cell with an alternative potential signal and observe how the system follows the perturbation at a steady state by measuring the current through the cell (Figure 14a). The electrochemical response is depended on several factors such as geometric heterogeneities (surface roughness) and chemical heterogeneities (surface-bound impurities).[62] The experimental data can be represented in the Nyquist plot (where the real vs. imaginary impedance components are plotted (Figure 14b).

$$Z = \frac{E_t}{I_t} = \frac{E_0 \sin(\omega t)}{I_0 \sin(\omega t + \phi)} = Z_0 \frac{\sin(\omega t)}{\sin(\omega t + \phi)}$$

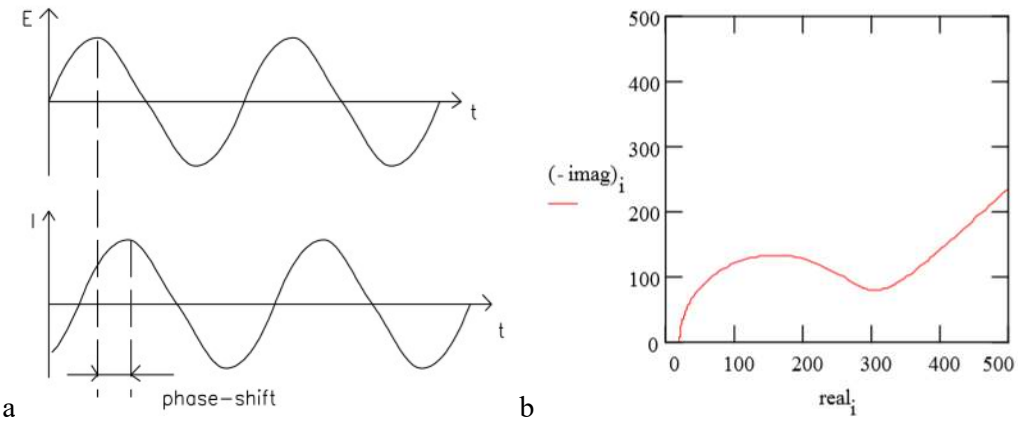

Figure 14. a) Sinusoidal Current Response in a Linear System b) Nyquist diagram.[63]

EIS experimental data is commonly analyzed by fitting it to an equivalent Randles circuit. It includes a solution resistance (R_s), a double layer capacitor (C_{dl}), charge transfer resistance (R_{ct}) and Warburg impedance (W) as shown in Figure 15.[63]

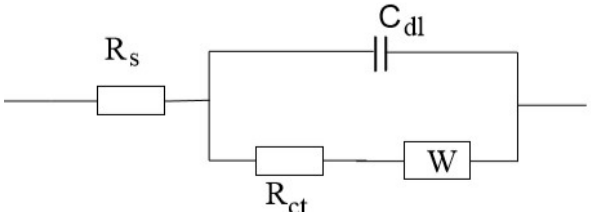

Figure 15. Randles Cell: Equivalent Circuit.

Warburg impedance indicates the impedance of electrons due to the diffusion interface between the bulk solution and the electrode interface. C_{dl} is the double-layer capacitance at the electrode interface formed as ions from the solution "stick-on" the electrode surface. The small separation between this charged electrode and the charged ions present in the electrolyte (often on the order of angstroms) forms the capacitor. R_{ct} refers to the resistance to electron transfer occurring due to the redox reaction at the electrode interface. The electrons enter the metal and metal ions diffuse into the electrolyte and vice-versa.

$$Me \Leftrightarrow Me^{n+} + ne^{-}$$

2. Experimental Methods

2.1 Reagents and Materials

Palladium (II) Chloride ($PdCl_2$, <99.99%, metals basis, Pd 59% min crystalline), Poly (vinyl pyrrolidone) (PVP Mol wt. 40,000, Sigma- Aldrich), Concentrated Hydrochloric acid (Conc. HCl, Himedia, 35% pure, Hi-AR), 4- Nitrophenol ($C_6H_5NO_3$, Sigma Aldrich, >99%), 2-Nitrophenol ($C_6H_5NO_3$, Honeywell, >99%), 2-Hydroxy-5-nitrobenzaldehyde ($C_7H_5NO_4$, Sigma Aldrich, 98%), 3- Nitrophenol ($C_6H_5NO_3$, Sigma Aldrich, >99%), 4-Nitroaniline ($C_6H_6N_2O_2$, Sigma Aldrich, >98%), Sodium borohydride ($NaBH_4$, Fluka Analytical,>99%), Absolute ethanol (C_2H_5OH, Ensure ACS, ISO, Reag.Ph Eur), Isopropanol (C_3H_8O, Merck, 99%), Hexane (C_6H_{14}, Rankem LR), Ethyl acetate ($C_4H_8O_2$, Rankem LR), Silica Gel (SiO_2, 100-200 mesh, Merck), Aluminium oxide active, neutral (Al_2O_3, 70-230 mesh, Himedia), Potassium carbonate anhydrous (K_2CO_3 anhy.99%, Extra pure, Loba Chemie), Phenyl boronic acid ($C_6H_7BO_2$, Alfa Aesar,98%),4-Iodotolulene ($CH_3C_6H_4I$, Alfa Aesar,98%). All the chemicals were used without further purification. The distilled water was taken from the Milli-Q purification system with specific resistance 18.2 MΩ cm.

2.2 Preparation of Pd nanocatalysts

Pd NCs stabilized by Poly(vinylpyrrolidone) (PVP) were synthesized using hydrothermal synthesis in five different solvent mixtures of Ethylene glycol (EG) and water. The synthesis has been described schematically in Figure 16. First, EG and water were mixed to prepare 30 mL solutions of 0 %, 25 %, 50 %, 75 %, 100 % volume by volume (v/v) of EG in water. For a typical synthesis, 2 g PVP (Mol Wt. = 40,000) was dissolved in 20 mL solvent in a 50 mL beaker by magnetic stirring at 1500 rpm until a clear solution is obtained (Figure 17a). Meanwhile, Palladium (II) Chloride (45 mg) is taken in an Eppendorf tube and conc. HCl (11 M, 250 µL) was added to it followed by ultrasonication for 10 min to convert it to H_2PdCl_4. This is transferred to another beaker and dissolved in 10 mL of solvent aided by ultrasonication (Figure 17b). H_2PdCl_4 solution was slowly added dropwise to the PVP solution under magnetic stirring and further stirred for 20 minutes to ensure homogeneity. The resulting brown solution (Figure 17c) was transferred into a 48 mL

Teflon-lined stainless autoclave (Figure 17d), kept in a preheated oven at 200 °C for 12 hours.

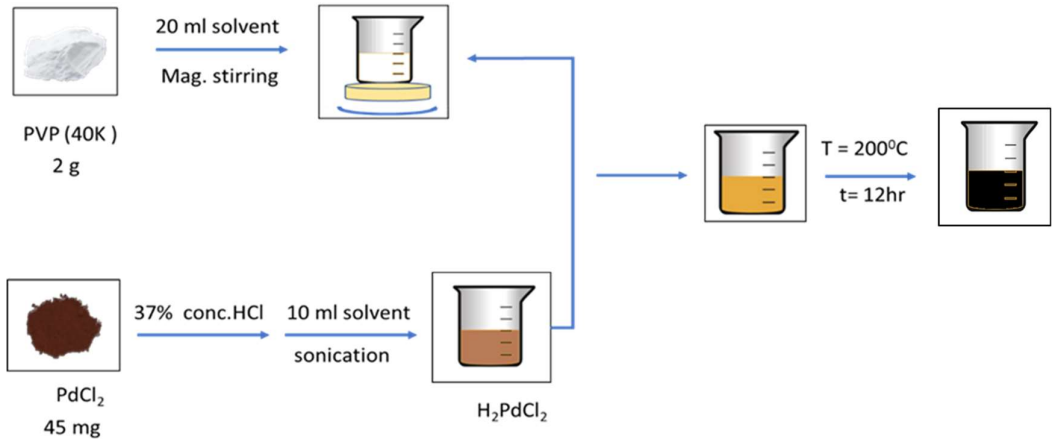

Figure 16. Schematic for synthesis of PdNCs

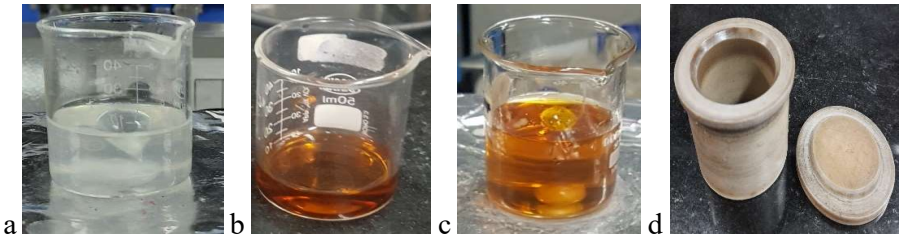

Figure 17. a) PVP solution, b) H_2PdCl_4 solution, c) resulting mixture, d) 48 ml autoclave.

Once the reaction was completed, the autoclave was cooled to room temperature and the black solution (Figure 18a) was obtained. Pd NCs were recovered by washing with water 5 times and then with ethanol 2 times to remove unreacted reagents and the excess PVP. For washing, the solution was sonicated for 15 minutes and then centrifuged at 13,500 rpm for 30 minutes (Figure 18b). Finally, the precipitates of Pd NCs were redispersed in 2ml ethanol. The ethanol dispersion of Pd NCs is stable for several weeks.

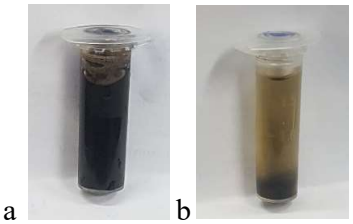

Figure 18. a) Obtained Pd NCs solution, b) Pd NCs solution after centrifugation

2.3 Materials characterization

Samples of as-synthesized Pd NCs were prepared for TEM analysis by pipetting diluted ethanol dispersion of Pd NCs onto a Formvar – coated, copper TEM grids. The drop casted

grids were kept in the vacuum desiccator for 30 min until complete solvent evaporation before imaging. The TEM data of the samples were obtained using a JEOL F200 TEM operating at 200 kV and processed using either Digital Micrograph or ImageJ 14.1 software. The histograms of the Pd NCs are obtained by measuring the diameter of at least 500 NCs. The average particle size (quoted as mean ± standard deviation) were calculated.

Powder X-ray diffractograms have been measured with a Rigaku Ultima IV diffractometer with Cu Kα X-Ray radiation (generator power setting: 40mA and 40kV) at a scanning rate of $2°min^{-1}$. Samples were prepared simply by drop-casting Pd dispersion in ethanol at the center of the glass coverslip and letting the solvent evaporate. The particle size was estimated from broadening of XRD reflections employing Scherrer formula given by

$$d = \frac{K\lambda}{\omega \cos\theta}$$

where d is the particle size (nm), λ is the X-ray wavelength (A°) of the radiation, θ is the angle of the considered Bragg reflection, w is the width (radians) on a 2θ scale, and K is a constant that depends on factors such as the geometry of the crystallites, which is here taken as 0.9.

FTIR spectra were recorded on a Perkin Elmer spectrometer between 700 and 4000 cm^{-1}. The samples were prepared by drying the Pd NCs dispersion in ethanol overnight, followed by mixing with KBr powder to form a pellet. The reference spectrum of pure PVP was also recorded.

2.4 Suzuki-Miyuara cross-coupling reactions

In a typical synthesis as shown in Figure 19a, phenylboronic acid (1.2 mmol), 4-iodotolulene (1 mmol) and K_2CO_3 (2 mmol) were taken in a 10 mL round-bottomed (RB) flask followed by addition of 4 mL ethanol/water (1:1,v:v) and 100 µL of Pd NCs dispersion in ethanol (0.01 mg/µL). The reaction mixture was stirred at 700 rpm at room temperature (T = 26±1°C). The progress of the reaction was monitored using thin-layer chromatography technique (TLC). At arbitrary time intervals,$\sim 100\ \mu L$ aliquot of the reaction mixture was taken in an Eppendorf tube, to which 2 drops of water and then 2 drops of ethyl acetate were added. Two separate layers can be observed, where the upper layer of ethyl acetate contains the reactant 4-iodotolulene and the biaryl product (if formed). Using a capillary tube, the upper organic layer was spotted on a TLC plate and ran through hexane as the mobile phase. The TLC plate was visualized under the UV chamber to check

the formation of the product. In the beginning, we can observe one spot corresponding to the reactant. As the reaction progress, the intensity of the spot corresponding to reactant diminishes and a new spot corresponding to the product is observed. The reaction was continued until a single spot was obtained in TLC (Figure 19b). The absence of additional spot was considered as the absence of any impurity.

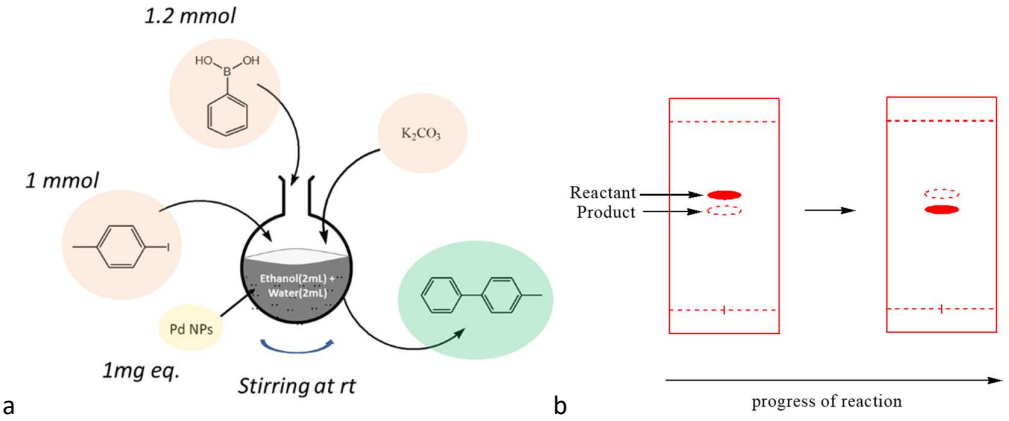

Figure 19. a) Schematic representation for Suzuki C-C coupling reaction
b) TLC monitoring of the progress of the reaction

After completion of the reaction, ethanol present in the reaction mixture was evaporated using a rotary evaporator. The obtained solution was taken in separating funnel and solvent extraction of the product was carried two times using ethyl acetate and water solvents. The lower aqueous layer which also contained the catalyst was discarded. The upper organic ethyl acetate layer was collected and evaporated using a rotary evaporator to obtain the required biaryl compound. The product was further purified using column chromatography. The column was packed with silica gel (SiO_2) and alumina (Al_2O_3) and ran down using hexane as eluent. The product was collected and was rota-evaporated to remove the solvent. The final product was dried under vacuum and analyzed through NMR using $CDCl_3$ as a solvent. The efficiency of the catalyst was evaluated by computing turn over frequency (TOF), where TOF can be defined as the moles of product formed per moles of catalyst atoms per second given below:[64]

$$\text{TOF} = \frac{moles\ of\ product}{moles\ of\ catalyst \times time\ (sec)}$$

Where moles of the product is given by yield times the moles of the substrate (here 4-iodotolulene) taken. For 1 mg of Pd NCs (Molar mass = 106.42 g/mol) ,

$$\text{number of moles} = \frac{10^{-3}\text{g}}{106.42\ g/mol} = 9.4 \times 10^{-6}\ \text{moles}$$

We further define surface turn over frequency (s-TOF) as a number obtained by dividing TOF by fraction of surface atoms. It indicates the number of molecules reacted at each available catalytic site per time, assuming that the number of active catalytic sites is equal to the total number of surface atoms.[65]

$$\text{Surface TOF} = \frac{\text{TOF}}{\text{The fraction of surface atoms}}$$

For estimation of the number of surface atoms, an ideal spherical shape for the nanoparticles was considered as an approximation.[66] From the total number of atoms present within a spherical nanoparticle, the number of atoms below the surface layer of the sphere was subtracted. The number of atoms within a sphere is obtained by calculating the volume of the sphere from the radius using the volume formula, then multiplying the volume by the density of the metal to give the mass of the nanoparticle. The mass was converted to moles and finally to the number of atoms using Avogadro's number.

$$\text{No. of atoms} = \frac{\text{density}\left(\frac{\text{g}}{cm^3}\right) \times \text{volume}(cm^3) \times \text{N}_\text{a}\,(\frac{atoms}{mol})}{\text{atomic mass}(\frac{g}{mol})}$$

To estimate the number of atoms below the surface layer of the sphere, the subsurface radius '$r_{subsurface}$' was defined which would be equal to the nanoparticle radius minus one diameter of a Pd atom. The covalent radius of the Pd atom is 0.138 nm, so a nanoparticle with radius 'r' would have a subsurface radius, $r_{subsurface}$ = r – 2 x 0.138 nm. The number of subsurface atoms is calculated by using the same formula but using the subsurface radius '$r_{subsurface}$' instead of radius 'r'. The number of surface atoms is the difference between the two.

For example, considering a 6.4 nm Pd nanoparticle, then

$$\text{Number of atoms} = \frac{12.023\left(\frac{\text{g}}{cm^3}\right) \times \frac{4}{3}\Pi(6.4\times10^{-7}cm)^3 \times 6.02\times10^{23}(\frac{atoms}{mol})}{106.42(\frac{g}{mol})}$$

$$= 9.16\times10^3$$

$$\text{r}_\text{subsurface} = 6.4\text{nm} - 2(0.138)\text{nm} = 6.12\times10^{-7}cm$$

$$\text{Number of atoms below the surface layer} =$$

$$\frac{12.023\left(\frac{\text{g}}{cm^3}\right) \times \frac{4}{3}\Pi(6.12\times10^{-7}cm)^3 \times 6.02\times10^{23}(\frac{atoms}{mol})}{106.42(\frac{g}{mol})} = 6.98\times10^3$$

$$\text{Number of surface atoms } = 2.18 \times 10^3$$

$$\text{Thus, the ratio of surface atoms to total atoms} = \frac{2.18 \times 10^3}{9.16 \times 10^3} = 0.238$$

Similarly, the number of Pd atoms, surface atoms per NCs, and hence fraction of surface atoms are calculated for Pd NCs with mean diameter 7.9 nm, 9.8 nm, 12.1 nm, and 16.9 nm. This is tabulated in the following Table 1. The ratio of Pd surface atoms to total atoms is found to be 0.238, 0.196, 0.160, 0.130, 0.095 respectively for different sized Pd NCs synthesized in 0 %, 25 %, 50 %, 75 %, 100 % (v/v) of EG in water.

Table 1. The fraction of surface atoms of the synthesized PdNCs

%(v/v) EG in water	NC mean diameter (nm)	No. of atoms per NCs	No. of surface atoms per NCs	The fraction of surface atoms
0%	6.4	9.16×10^3	2.18×10^3	0.238
25%	7.9	1.73×10^4	3.39×10^3	0.196
50%	9.8	3.34×10^4	5.34×10^3	0.160
75%	12.1	6.53×10^4	8.84×10^3	0.130
100%	16.9	1.73×10^5	1.64×10^4	0.095

2.5 Catalytic reduction of nitroaromatics

Firstly, the dispersion of each of the synthesized Pd NCs in water (0.4 mg/mL) is prepared. For this, 1 mg of the dried Pd NCs is taken in a vial and is dispersed in 2.5 mL water by sonicating for about 2 h. The stock solutions of 4-nitrophenol, 3-nitrophenol, 2-nitrophenol, 2-hydroxy-5-nitrobenzaldehyde, and 4-nitroaniline are prepared in water. The aqueous solution of 0.3 M sodium borohydride ($NaBH_4$) is freshly prepared before taking measurements.

In a standard quartz cuvette of path length 1 cm, 2.7 mL nitro-substrate solution is mixed with 0.3 mL $NaBH_4$ (0.3 M) solution at room temperature (T = 26±1°C). To this, a fixed volume of each of the different Pd NCs dispersion solution (0.4 mg/mL) was added and mixed. The concentration of the nitro-substrate and amount of Pd NCs were optimized so that starting absorbance value lies between 1 and 2 and allows facile comparison of catalytic efficiency of the various synthesized Pd NCs. The different concentrations of the various nitro-substrate solution and different volumes of Pd NCs tested are summarized in Table 2.

Figure 20 shows the schematic representation of the catalytic reduction of nitro-aromatic compounds.

Table 2. Catalytic reduction by Pd NCs for various conditions

Nitro- substrate	Concentration of the nitro-substrate	Pd cat. (0.4 mg/mL) loading volume (µL)
4- Nitrophenol	0.1 mM	10 µL
3- Nitrophenol	0.5 mM	9 µL
2- Nitrophenol	0.5 mM	9 µL
2-hydroxy-5-benzaldehyde	0.1 mM	10 µL
4-nitroaniline	0.2 mM	6 µL

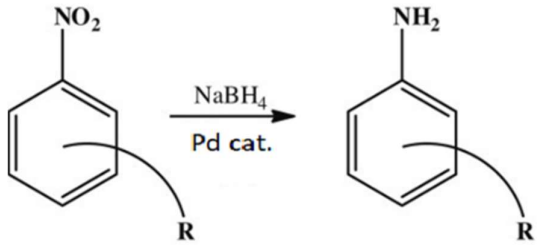

Figure 20. Catalytic reduction of nitro-aromatic compounds

The cuvette was placed inside a UV-VIS spectrophotometer and the reaction was monitored by recording the changes in the absorption spectra with time. As the reaction progressed, the bright yellow solution gradually became colourless. In the reaction medium, sodium borohydride concentration seems to be much higher than that of nitro-substrate and remains essentially constant during the course of the reaction. As a result, the reduction rate is independent of the concentration of $NaBH_4$. Accordingly, the nitroaromatic reduction is considered to be a pseudo-first-order reaction and the rate constant is determined using pseudo-first-order kinetics.

The apparent rate constant, k was calculated by following the first-order rate law:

$$\ln\left(\frac{A_t}{A_0}\right) = -kt$$

Where A_o and A_t are absorbance values (at 420 nm) representing the reactant concentrations in the beginning and at time t respectively.

TOF was calculated according to the equation, similar to Suzuki-Miyuara coupling reaction:

$$\text{TOF} = \frac{moles\ of\ product}{moles\ of\ catalyst \times time\ (sec)}$$

Surface turn over frequency (s-TOF) is obtained by dividing TOF by fraction of surface atoms, assuming that the number of active catalytic sites is equal to the total number of surface atoms.[65]

$$\text{Surface TOF} = \frac{\text{TOF}}{\text{The fraction of surface atoms}}$$

2.6 Electrochemical Measurements

The measurements were performed at room temperature using an electrochemical workstation (CHI760E) in a 3-electrode arrangement with Ag/AgCl as a reference electrode and Pt wire as the counter electrode in neutral medium (Figure 21). The working electrode was prepared by drop-casting 10 µL of Pd NCs on a glassy carbon electrode of 3mm diameter. The glassy carbon electrode was polished with 0.05-micron and 0.5-micron alumina powder and cleaned by ultrasonication in water and isopropyl alcohol to get a mirror finish surface. Pd NCs solution was prepared by mixing of 0.25mg Pd NCs (dispersion in ethanol) in 100µL of Nafion: isopropanol: water (in ratio 0.5:1:4,v:v:v) solution by ultrasonication. Impedance measurements were performed in 1mM $K_3[Fe(CN)_6]$ with 0.1 M KCl as supporting electrolyte within a frequency range of 1000KHz to 1000Hz with AC voltage amplitude of 10mV at open circuit potential (V_{oc}= 0.31V). The obtained data were fitted into the Randles equivalent circuit model (as discussed in the introduction section).

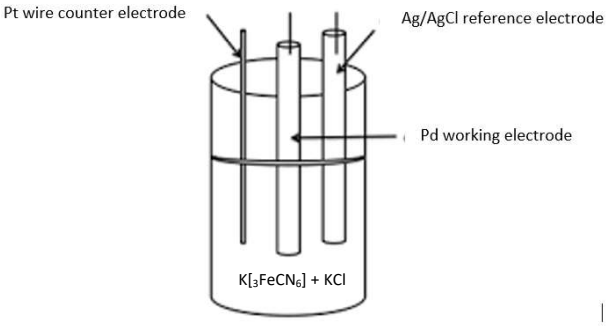

Figure 21. Schematic representation of an electrochemical cell for impedance measurements

3. Results and discussion

3.1 Synthesis and characterization of the Pd NCs

A. TEM Characterization

TEM images and corresponding size histograms (Figure 22) show that the size of Pd NCs synthesized using the solvothermal method is depended on the composition of the solvent used. All these Pd NCs have quasi-spherical shapes and are crystalline in nature as revealed by the presence of lattice fringes. The electron diffraction pattern displaying diffuse rings can be indexed on the (111), (200), (220), (311), (331) diffraction planes respectively of fcc-Pd.

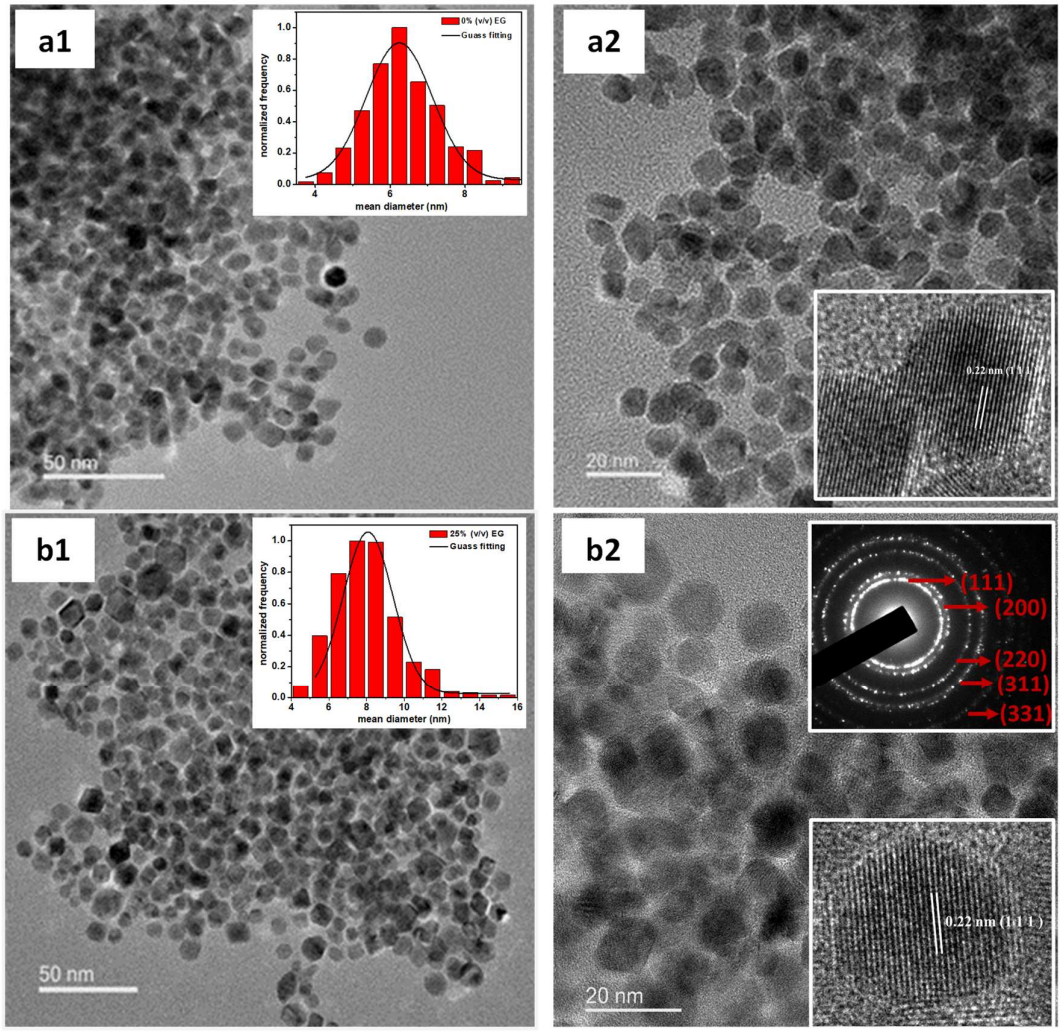

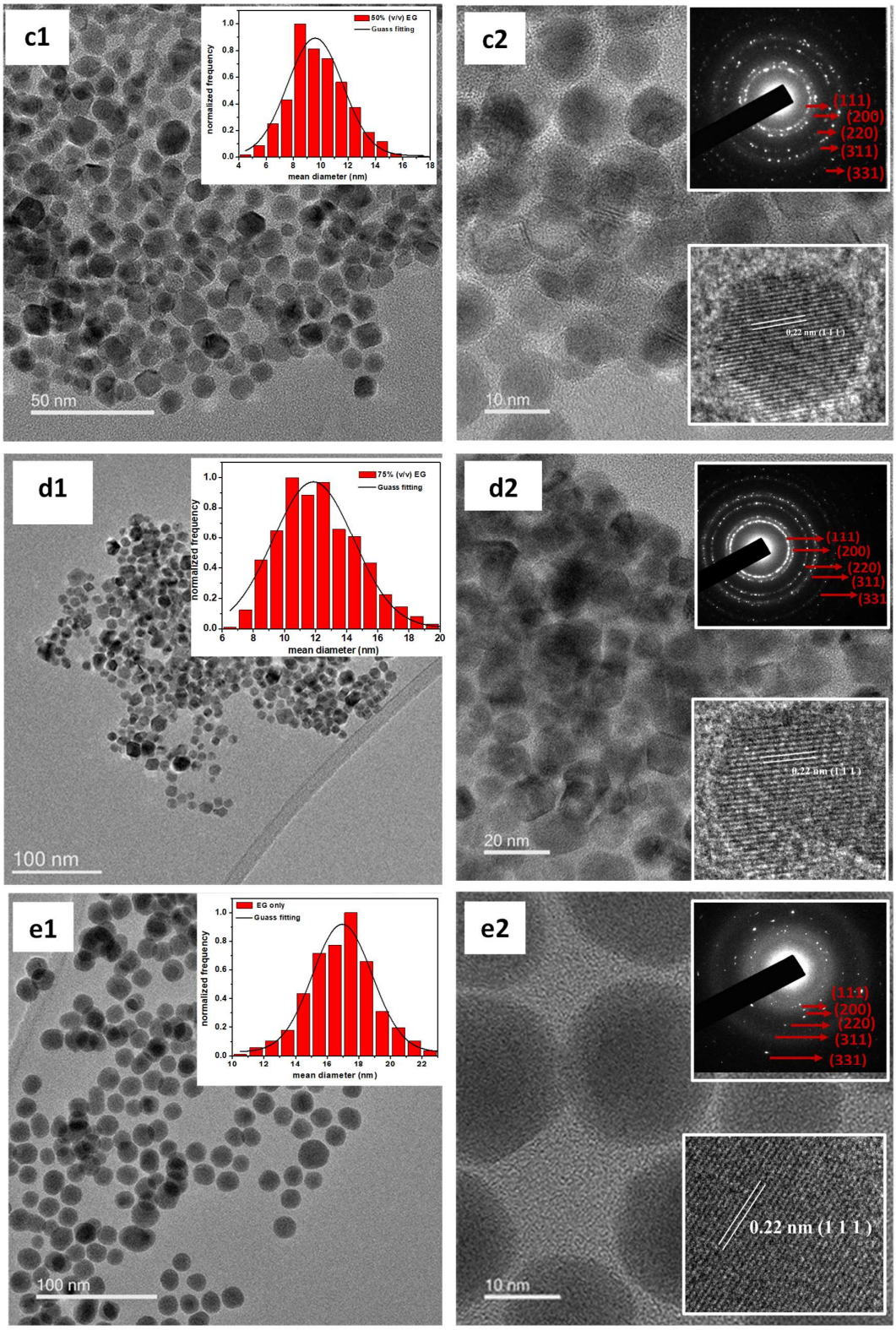

Figure 22. Representative TEM images a1, b1, c1, d1 and e1 of the Pd NCs synthesized in 0 %, 25 %, 50 %, 75% and 100 % (v/v) of EG in water respectively (insets are the corresponding size distribution histogram). a2, b2, c2, d2, and e2 are the closer view of Pd NCs respectively with corresponding SAED pattern and HR-TEM images as inset.

Interestingly, the average nanoparticle size gradually increases with increasing the fraction of EG in the solvent mixture as shown in Figure 22. The particle size distribution (PSD) histograms (Figure 22), demonstrated that Pd NCs were nearly monodisperse with average size of 6.4 ± 1.1, 7.9 ± 1.6, and 9.8 ± 2.1, 12.2 ± 2.4, 16.9 ± 2.3 nm respectively for 0 %, 25 %, 50 %, 75 %, 100 % (v/v) of EG in water as solvent of synthesis. In Table 2, mean diameter size (D_{avg}) and relative standard deviation (σ_r %) of the Pd NCs synthesized in the varying composition of EG in water are presented.

Table 3. The size distribution of the Pd NCs synthesized in solvent mixtures of H_2O-EG.

%(v/v) EG in water	D_{avg} (nm)	σ_r (%)
0 %	6.4	17
25 %	7.9	20
50 %	9.8	21
75 %	12.1	20
100 %	16.9	13

Table 3 reveals that nanoparticle size is related to the viscosity, dielectric constant, and boiling point of the solvent mixtures as determined by the fraction of ethylene glycol. Lesser is the fraction of EG in water, the boiling point of the solvent mixture is found to be lower, and consecutively particle size of Pd NCs also decreases.[36,37] A similar correlation between viscosity and particle size has also been observed.[30,36] The increasing viscosity of the H_2O-EG mixture leads to a bigger nanoparticle size. These can be attributed to a slower nucleation rate in highly viscous, high boiling solvents. Greater viscosity limits collision of species and a thus small number of nuclei formation, leaving more precursor left for growth and hence larger sized nanoparticles are formed. The solvent mixture also determines the reducing ability of the Pd precursor. The dielectric constant of the solvent can change the reactivity of reducing agents and precursors and stability of nuclei.[28] In solvents with a higher fraction of water, i.e. greater dielectric constant, reduction pathway of metal precursor gets accelerated since they tend to stabilize ions.[21,24,28] Because of a large number of nuclei formation, little is left for subsequent growth. This explains why smaller size nanoparticles are obtained with increasing water during synthesis. Figure 23 depicts the general trend observed.[67–70]

Table 4. Solvent properties of H_2O- EG mixtures

Sample	%(v/v) of EG in water	NC size (nm)	BP[67] (°C)	Viscosity[68] (mPa s) at 297 K	Dielectric constant[69,70] (at 20° C)
S1	0%	6.4	100	0.91	80
S2	25%	7.9	103	3.69	74
S3	50%	9.8	107	7.61	64
S4	75%	12.1	123	12.3	55
S5	100%	16.9	197	19.1	42

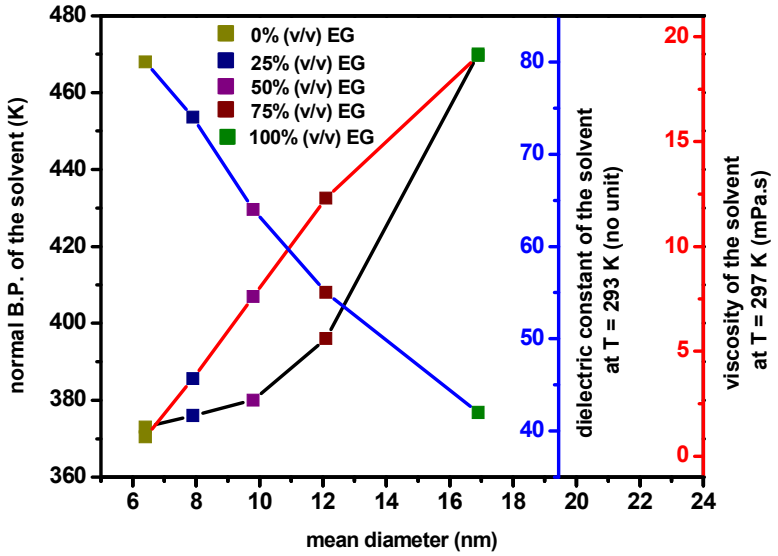

Figure 23. A general correlation between size and solvent properties of the H_2O-EG mixture a) normal boiling point b) viscosity at T=297 K c) dielectric constant at T=293 K.

Another way of explaining increasing particle size with increasing ethylene glycol is in terms of different capping ability of PVP in different solvents and thus different growth rates. By changing the nature of the solvent, PVP surfactant solvation and hence its strength and range of PVP-PVP interactions will get significantly impacted.[20,46,50] This can be verified by taking Hansen interaction parameters into account, which is an energy density based on dispersion bonds (δ_D), polar bonds (δ_P), and hydrogen bonds (δ_H).[71] R_a is the distance between Hansen parameters (δ_D, δ_P, δ_H) in Hansen space between solute '1' (here PVP) and solvent '2'. This helps in determining the interaction parameter $\chi_{1,2}$ which provides a measure of the thermodynamic affinity of the solvent to the polymer, given by the following equations.

$$R_a = [4.(\delta_{D1} - \delta_{D2})^2 + (\delta_{P1} - \delta_{P2})^2 + (\delta_{H1} - \delta_{H2})^2]^{1/2}$$

$$\chi_{1,2} = \frac{V_s.{R_a}^2}{RT}$$

Index 1 and 2 denote the ligand and the solvent. V_s is the molar volume of the solvent. R and T are the ideal gas constant and the temperature. According to Hansen approach, a larger Ra value thus larger $\chi_{1,2}$ suggests stronger attraction between the ligands due to the surrounding solvent.[20] From Table 3, it can be observed that a fraction of EG in water is increased, Ra parameter (between PVP and solvent) becomes smaller.[71] This implies that ligand−ligand attraction becomes weaker with increasing fraction of EG and hence decreasing the rigidity of the ligand layer around Pd NCs. Due to fact that the presence of PVP ligand layer around Pd crystal nuclei during growth step hinders their growth of the crystal, the increasing stability of the ligand layer will restrict the final size of the nanoparticle as observed in experimental results.[48,72] For nanoparticles synthesized in water, PVP-PVP interactions are much stronger resulting in a more rigid ligand layer during the growth step; therefore particle size gets restricted to a greater extent.

Table 5. Correlation between Hansen solubility parameter and nanoparticle size

Sample	%(v/v) of EG in water	R_a(solvent/PVP)	NC diameter (nm)
S1	0%	28.7	6.4
S2	25%	24.4	7.9
S3	50%	20.1	9.8
S4	75%	15.8	12.1
S5	100%	11.4	16.9

B. XRD Characterization

From the X-ray diffraction study (Figure 24), the formation of pure Pd metallic particles was confirmed. The profile shows three intense sharp peaks for Pd synthesized, which can be assigned respectively, to (111), (200), (220) planes of face-centered cubic (fcc) lattice of palladium. It is indicated that crystallite size gets bigger as the composition of EG during synthesis is varied from 0%, 25%, 50% 75% to 100%.

The apparent average crystallite size of metal nanoparticle was calculated by considering the full width at half maximum (FWHM) of (111) peak using the Debye -Scherrer equation (Table 6). These are found to be 5.2 nm, 6.0 nm, 7.3 nm ,8.1 nm, 8.6 nm respectively for nanoparticles synthesized from 0%, 25%, 50%, 75% and 100% EG.

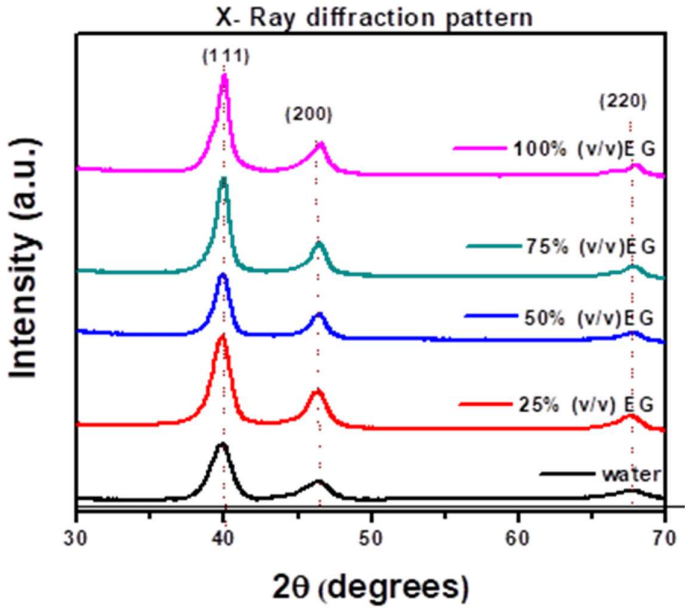

Figure 24. PXRD pattern of Pd NCs synthesized in 0%, 25%, 50%, 75%, 100% (v/v) of EG in water.

Table 6. Calculation of crystallite size using (111) facet

Sample code	%(v/v) EG in water	2θ (degrees)	FWHM (degrees)	The crystallite size (nm)
S1	0% EG	39.90°	1.62°	5.2 nm
S2	25% EG	39.86°	1.42°	6.0 nm
S3	50% EG	39.92°	1.16°	7.3 nm
S4	75%EG	39.96°	1.04°	8.1 nm
S5	100% EG	40.02°	1.00°	8.6 nm

C. FTIR Characterization

Figure 25 shows a series of FTIR spectra of Pd NCs prepared with different compositions of EG-H_2O solvent mixtures and pure PVP between 1000 and 4000 cm^{-1}. It can be observed that the FTIR spectra of pure PVP are similar to the samples. This shows that even after several washing steps by water and ethanol, PVP entirely surrounds catalyst surface forming an organic multi-layer shell irrespective of the composition of solvent used during Pd NCs synthesis. For pure PVP spectra (Table 7), the absorption band located around 1660 cm^{-1} can be ascribed to the stretching vibration of the C=O in the pyrrolidone group. Secondly ,the CH stretching modes can be assigned to five overlapping signals :asymmetric

CH_2 stretching (ring : 2953 cm^{-1} , chain: 2983 cm^{-1}) , symmetric CH_2 stretching (chain 2919 cm^{-1} , ring :2885 cm^{-1}) and ternary CH (2852 cm^{-1}). The bands at 1427cm^{-1} and 1371 cm^{-1} also correspond to CH deformation modes from the CH_2 group. Also, absorption bands at 1286 cm^{-1} which is due to C-N bending vibration from the pyrrolidone structure can be noticed. Since PVP is bi-substituted amide absorptions bands of amines (3400-3500 cm^{-1}) are not observed.[72]

Table 7. FTIR characterization peaks for PVP

FTIR peak (cm^{-1})	Vibrational mode[72]
1660 cm^{-1}	C=O stretching
2953 cm^{-1}	Asymmetric $\nu(CH_2)$ of ring
2983 cm^{-1}	Asymmetric $\nu(CH_2)$ of chain
2919 cm^{-1}	Symmetric $\nu(CH_2)$ of chain
2885 cm^{-1}	Symmetric $\nu(CH_2)$ of ring
2852 cm^{-1}	Ternary ν(CH) of chain
1427 , 1371 cm^{-1}	CH deformation mode from CH_2 group
1286 cm^{-1}	Bending stretch ν(N-H)

In the case of FTIR spectra of the catalysts, the intensities of the absorption bands from residual PVP are not very significant as compared to those of pure PVP because of the successful removal of weakly adsorbed PVP by washing. However, the main absorptions bands for Pd NCs like the C=O group can still be identified. The washed Pd NCs show clear C=O stretching band at around 1641 ,1641 ,1637 , 1633 , 1577 cm^{-1} respectively for samples prepared with solvent composition 100%(v/v), 75%(v/v) , 50%(v/v) , 25%(v/v) , 0%(v/v) of EG in water . These redshifts observed for catalysts as compared to pure PVP suggests strong chemisorption of C=O on the surface of Pd NCs, which decreases the electron density in the carbonyl bond and thus the vibration energy. The partial donation of oxygen lone pair to Pd causes -C=O peak to split into two peaks centered at around 1633 cm^{-1} and 1577 cm^{-1}, although the intensity ratio varies depending on the interaction. It is observed that in the case of 0% (v/v) EG in the water sample, the lower wavenumber peak is noticeable while for the rest, the other peak is visible. The extent of redshifts depends hugely on the surface coverage density of PVP around the catalyst.[72] It is likely that for the samples where retained PVP forms a thicker layer around the catalyst surface, redshift is

less noticeable.[72] Thus it is predicted that with increasing fraction of EG in the solvent mixture during synthesis, PVP shell around washed catalyst becomes denser.

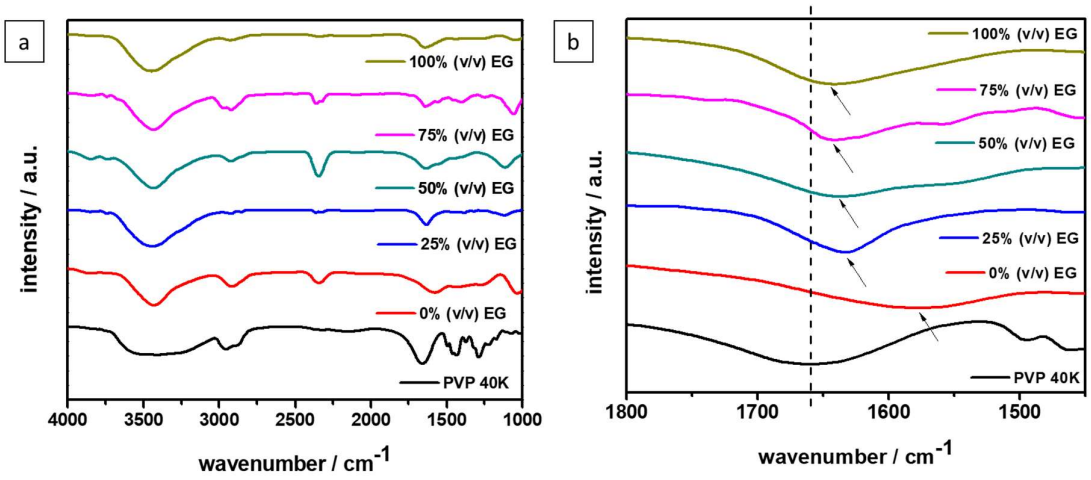

Figure 25. a) FTIR spectra of Pd NCs synthesized in 0%, 25%, 50%, 75%, 100% (v/v) of EG in water as well as pure PVP in the range of 1000-4000 cm^{-1}. b) Zoom-in view of the FTIR spectra showing the C=O-Pd interaction between 1400-1900 cm^{-1}.

3.2 Catalytic activity for Suzuki-Miyaura cross-coupling reaction

To compare the catalytic efficiency of the synthesized Pd NCs, the nanocatalysts were applied to the Suzuki–Miyuara coupling reaction. Suzuki–Miyaura coupling represents one of the most valuable reactions for the formation of C-C bonds, characterized by many advantageous features including mild reaction conditions and the easy handling of reagents and byproducts.[57,60,73–76] The catalysts were evaluated for the Suzuki coupling reaction between 4-iodotolulene (1mmol) and phenylboronic acid (1.2 mmol), using K_2CO_3 (2mmol) as a base at room temperature in a benign water-ethanol (1:1) solvent mixture. We chose 4-iodoanisole over Bromo /Chloro- substituted substrates since the I-Ph bond has lower bond dissociation enthalpy, making the coupling reaction more feasible. Due to the increasing importance of green solvents in organic synthesis, the coupling reactions were carried in an aqueous-based solvent mixture, thus avoiding the traditionally used organic solvents, such as toluene or THF. The use of a mixed solvent escalates the reaction rate by increasing the solubility of the base and the reactants. Also, the poor solubility of the biphenyl compounds (product) in the aqueous-ethanol mixture apparently drives the reaction equilibrium forward. Under identical reaction conditions, the progress of the reaction was checked for 1mg Pd NCs dispersion in ethanol (0.8 mol%). The catalytic performance of PdNCs is summarized in Table 8.

Table 8. Suzuki- Miyaura cross-coupling reactions with Pd NCs

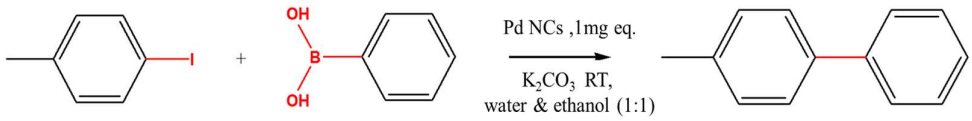

Sample	% (v/v) EG in water	Time (min)	Yield (%)	TOF(sec^{-1})	sTOF (sec^{-1})
S1	0% EG	25	95	6.74×10^{-2}	2.83×10^{-1}
S2	25% EG	45	90	3.55×10^{-2}	1.81×10^{-1}
S3	50% EG	90	95	1.87×10^{-2}	1.17×10^{-1}
S4	75% EG	180	95	9.40×10^{-3}	7.24×10^{-2}
S5	100% EG	420	60	2.50×10^{-3}	2.68×10^{-2}

It can be observed that with increasing % composition of EG in the solvent of synthesis, time taken for 90% completion of reaction too goes up. The reaction was rather efficient for sample S1 (PdNCs synthesized in water), achieving greater than 90% yield in less than 30 min (Table 8), while the results from sample S5 (Pd NCs synthesized in ethylene glycol) are not at all satisfactory.

The obtained NMR spectrum verifies the purity of the product .^{1}H NMR spectrum at room temperature shows six sets of peaks (Figure 26). The total number of protons was obtained by integrating the peaks and it was found to be 12, which corresponds to the total number of protons of the expected product. Singlet found around 2.42 ppm, with the integration of 3 which corresponds to that of the proton (a) as shown in the estimated Figure 27. Similarly, three doublets at 7.28 ppm ,7.52 ppm and 7.61 ppm, along with triplet at 7.45 ppm can be observed in range of 7-8 ppm. The multiplet at 7.33 ppm corresponds to (f) along with the trace amount of solvent.

Characterization Data of 4-methyl-1,1′-Biphenyl : White solid; ^{1}H NMR (500 MHz; CDCl3; δ, ppm): 7.28 (d, J = 8.5, 2H), 7.61 (d, J = 9.5 Hz, 2H), 7.52 (d, J = 9.5 Hz, 2H), 7.45 (t, J = 9.0 Hz, 2H), 7.36 (m, 1H), 2.42 (s, 3H).

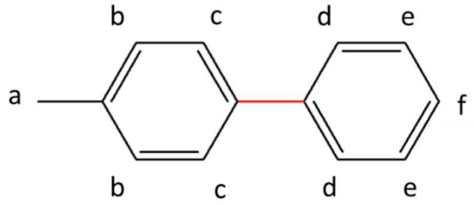

Figure 26. NMR characterization of the biaryl product

a: 3H, s, 2.425 ppm

b: 2H, d, 7.533,7.514 ppm

c: 2H, d, 7.617,7.598 ppm

d: 2H, d, 7.288,7.271 ppm

e: 2H, t, 7.472,7.454,7.436ppm

f: 1H, m,7.369,7.365,7.333,7.332ppm

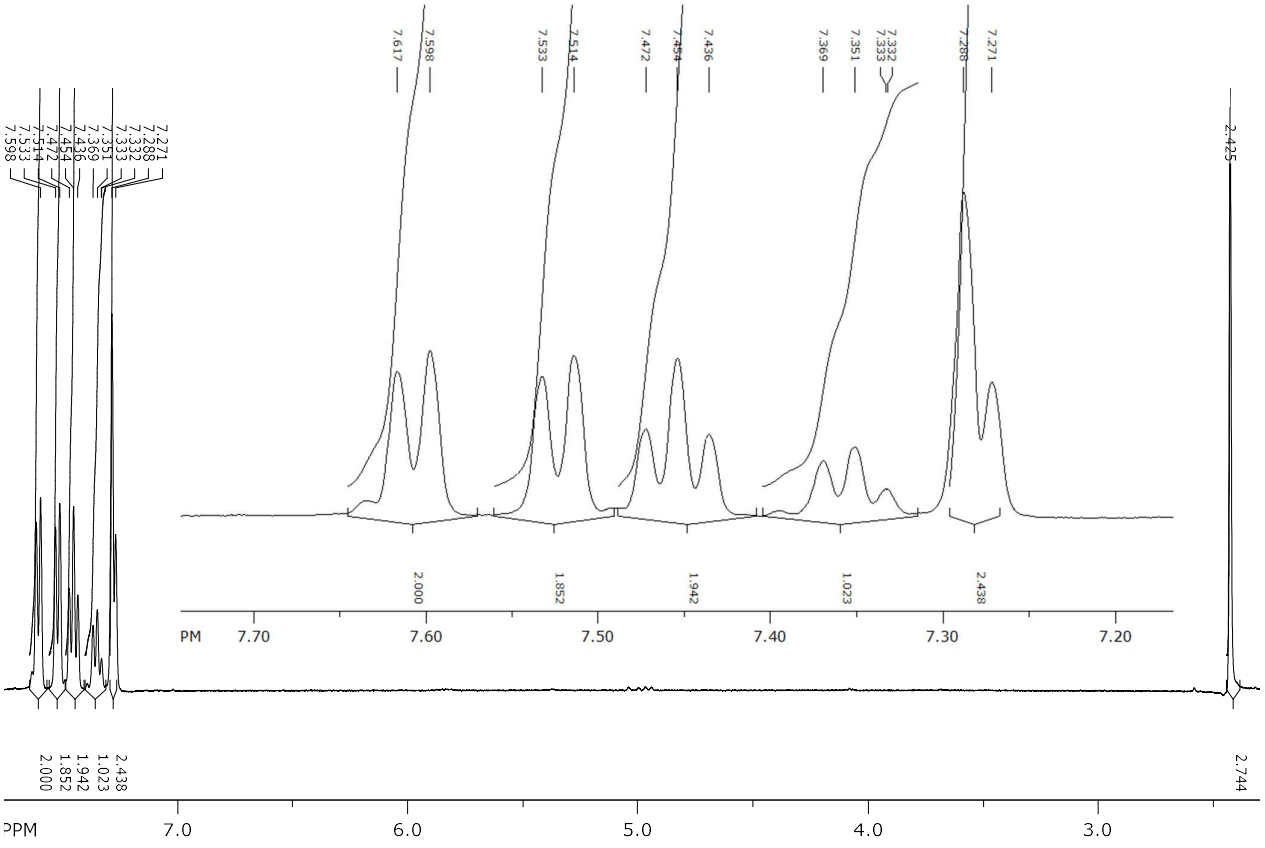

Figure 27. NMR spectra of the biaryl product.

Although it is observed that decreasing the size of PdNCs has favoured the reaction rate, further analysis showed that the relation between the size and reactivity is more complicated suggesting additional effects of the solvents used, not merely its size. In order

to understand the effects in detail, turn over frequency normalized to fraction of surface atoms (s-TOF) was calculated, as described in the experimental section. By definition, s-TOF should be a constant across a set of catalysts, assuming that only surface Pd atoms participate in a coupling reaction. There might be some deviation from the calculated s-TOF values as all particles may not be spherical as we have presumed. However, the different extent of deviation from a spherical shape is also an influence of the solvent of synthesis and commensurate with our goal of elucidating the solvent effect. The highest s-TOF value was observed to be 0.281 for sample S1 and the other samples were expected to show a similar value. What surprised us though was that s-TOF values were decreasing significantly from the highest value of ~0.281 to 0.181 for S2, 0.117 for S3, 0.072 for S4, and 0.027 for S5 (Table7). The differences in the s-TOF values are far larger than smaller variations in size or size distribution in the nanoparticles accounted for. Thus, there is a nearly 10-fold decrease in s-TOF values as the size of nanoparticles increased while synthesized in the presence of EG solvents (Figure 28). The experimental results have suggested that nanoparticles prepared in different solvents can have different surface properties and show different reactivities.

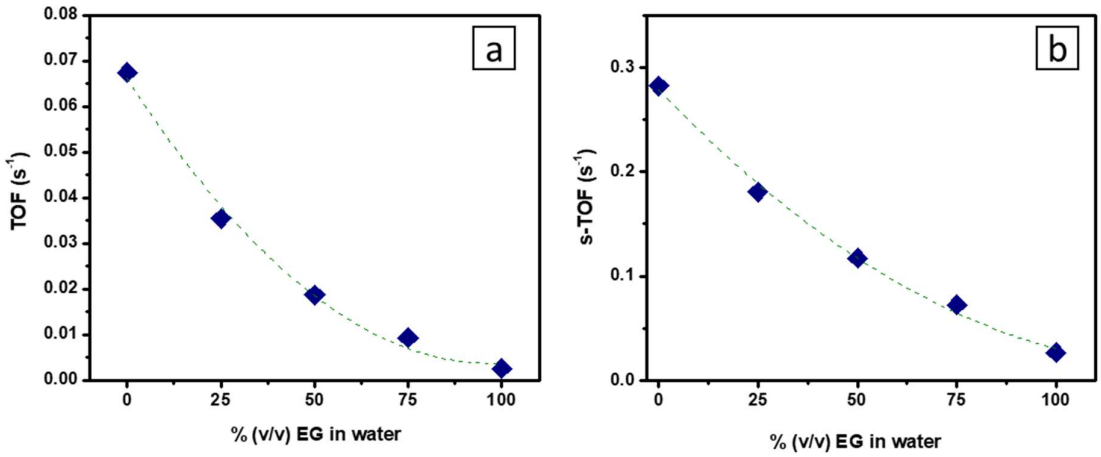

Figure 28. a) TOF and b) s-TOF of the synthesized Pd NCs in different solvent mixtures of H_2O-EG for the Suzuki-Miyuara coupling reaction.

The superior catalytic reactivity of the Pd NCs synthesized in water is probably a result of the higher surface energy. The disparity in the s-TOF has suggested that the interaction between the catalytic surface and the reactants vary depending on the composition of solvent mixtures used during synthesis. The interactions between the metal surface and ethylene glycol are seemingly stronger as compared to water. The strong metal surface-solvent interactions may prevent successive adsorption and activation of the reactant during

the reaction and produce a poisoning effect. As the fraction of ethylene glycol during synthesis would increase, the surface energy of the catalyst would deplete and thus leading to poorer catalytic performance.

3.3 Catalytic activity for reduction of nitroaromatics

The reduction of nitroaromatic compounds by borohydride ion on noble metal-based nanocatalysts has emerged as one of the most widely used model reactions for assessment of their catalytic activity[77–80]. This is because of the simplicity and ease through which the reaction can be monitored using spectroscopic techniques. The reaction occurs in water under ambient conditions, has no known side reactions, and will only proceed if a catalyst is present. Thus, for quantitative evaluation of the catalytic activity of the as-synthesized Pd NCs, apparent kinetic rate constant was calculated for the reduction reaction of several substates including 4-Nitrophenol (4-NP), 2-hydroxy- 5-nitrobenzaldehyde (2,5-NB), 2-nitrophenol (2-NP), 3-nitrophenol (3-NP) and 4- nitroaniline (4-NA). The following Figure 29-30 compares the apparent rate constant k_{app} (min^{-1}) of the different PdNCs synthesized in a) 0% b) 25% c) 50% d)75% e)100% (v/v) of EG in water for catalytic hydrogenation of the various nitro-substrates.

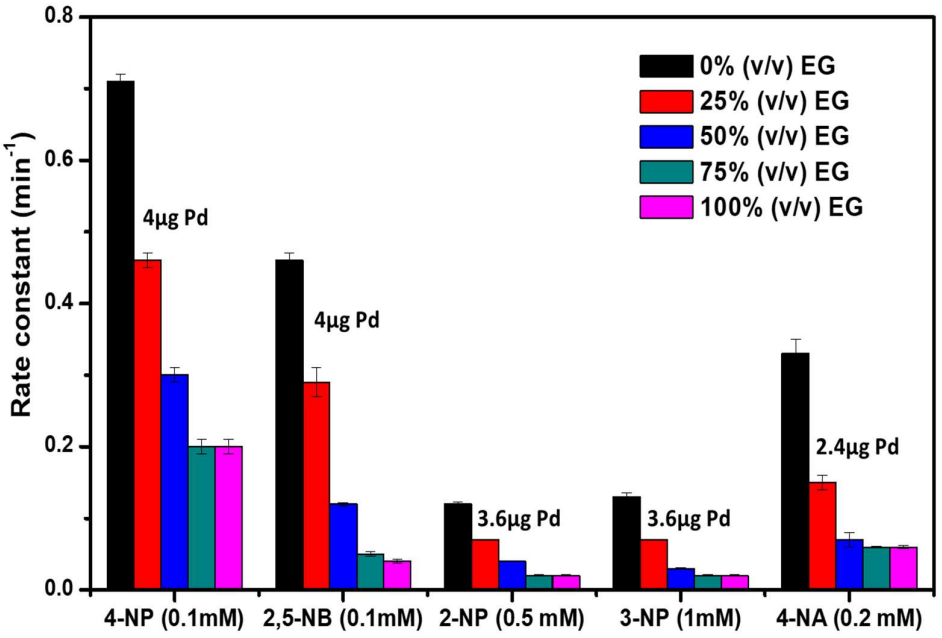

Figure 29. Comparison of the rate of catalytic hydrogenation activities

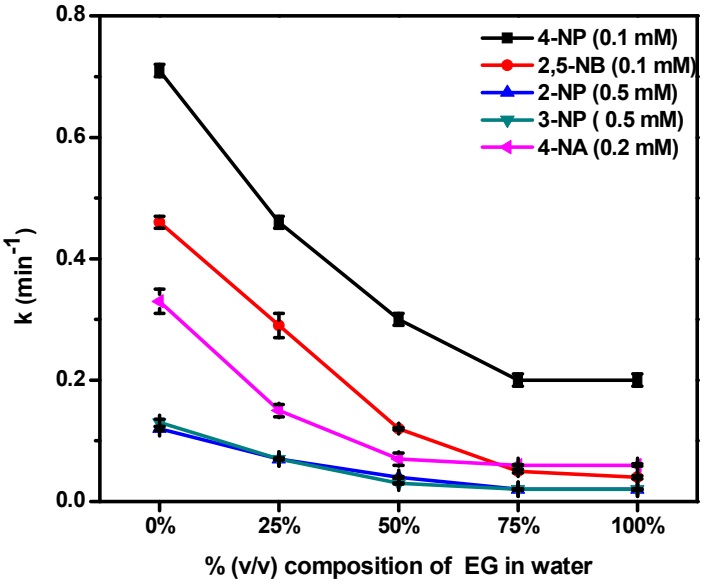

Figure 30. Rate constants for catalytic reduction for different sized PdNCs

Initially, we can observe a linear decrease in the kinetic rate constant with increasing size for range 6-10 nm where the solvent of synthesis is mostly water, but once the solvent composition of synthesis is dominated by ethylene glycol, the kinetic rate of hydrogenation begins to saturate and thus become independent of nanocatalyst size. In theory, the finer the Pd NCs size, the higher will be the specific surface area and faster will be the catalytic hydrogenation rate. However, in practice for finer particle coating of the palladium surface by the stabilizing agents (solvent, PVP, etc) may become a controlling factor. The experimental results show that rate constant though found to decrease with increasing size after a certain point size becomes an insignificant factor for determination of the catalytic efficiency. It indicates that the nature of the catalyst's surface (amount and orientation of stabilizers residing, surface defects, etc) is more influential. Owing to the physical properties of the ethylene glycol solvent (boiling point, viscosity, etc.), it is expected that EG would stick to catalyst surface much more strongly as compared to water. While the washing process of the PdNCs by the polar solvents water and ethanol may rejuvenate the otherwise passivated surface, it is greatly difficult to remove ethylene glycol residing on the catalyst surface.

The general trend suggests the possibility that ethylene glycol has poisoned the active sites of the nanocatalyst and is thus interfering with the steps involved in the reduction. The stabilizers prevent the facile diffusion of the reactant molecules towards the catalyst surface, therefore inhibiting their performance. For Pd NCs synthesized in water, the

surface atoms are much more accessible for catalysis due to efficient washing. Good adsorption of the substrates helps in promoting the reduction reaction. Greater the exposed surface area higher will be the electron transfer and thus higher will be the rate constant of catalytic reduction of the nitroaromatic compounds. This explains why the Pd NCs synthesized in only water showed excellent catalytic activity in the case of all these Ar–NO_2 substrates The following Table 9 compiles the rate constant for reduction of 4-NP as well as other nitro-aromatic compounds by Pd NCs synthesized in different solvent mixtures of H_2O-EG.

Table 9. Apparent rate constants for the nitro reduction

Sample	%(v/v) EG in water	Apparent rate constant (min^{-1})				
		4-NP	2,5-NB	2-NP	3-NP	4-NA
S1	0%	0.71	0.46	0.12	0.13	0.33
S2	25%	0.46	0.29	0.07	0.07	0.15
S3	50%	0.30	0.12	0.04	0.03	0.07
S4	75%	0.21	0.05	0.02	0.02	0.06
S5	100%	0.20	0.04	0.02	0.02	0.06

It can be observed that the catalytic activities for the reduction of nitroaromatic compounds are influenced by the solvent used for the synthesis. The rate constant values obtained show high catalytic efficiency of Pd NCs synthesized in water compared to PdNCs synthesized in solvents containing ethylene glycol. The trend is seen to be followed for all of the Ar-NO_2 substrates. In the following Figure 31a-b, relative TOF and s-TOF of different Pd NCs synthesized (w.r.t. TOF and s-TOF of Pd NCs synthesized in water respectively are plotted against % composition of H_2O-EG solvent mixture of synthesis. The difference in s-TOF confirms that the solvent of synthesis affects the catalytic performance of the Pd NCs. It is observed that Pd NCs synthesized in water shows the best catalytic activity. The s-TOF values are found to be significantly decreasing with increasing EG fraction for Pd NCs synthesized in ≤ 50 % (v/v) of EG in water. However, for >50% (v/v), the effect is much less pronounced.

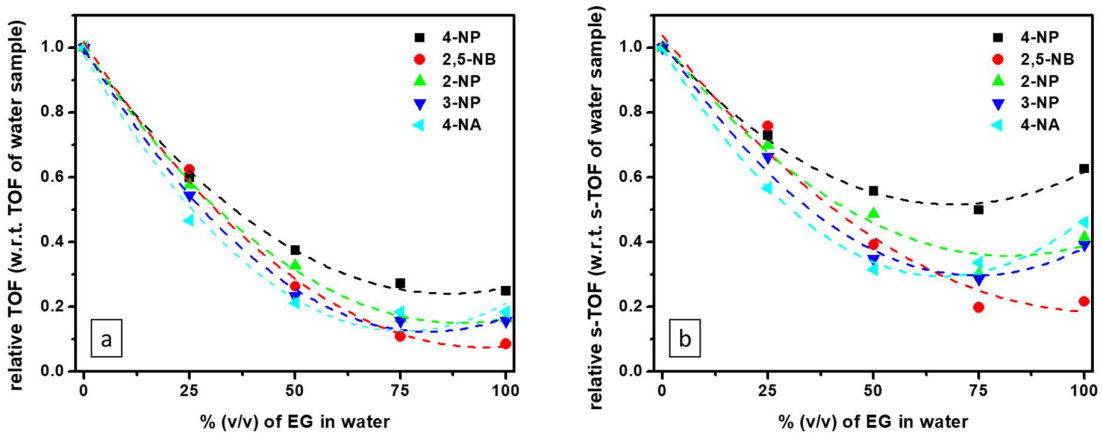

Figure 31. a) Relative TOF and b) relative s-TOF of the synthesized Pd NCs in different solvent mixtures of H_2O-EG (with respect to TOF and s-TOF of Pd NCs synthesized in water respectively) for the catalytic reduction of the various nitro-aromatic substrates.

A. 4-nitrophenol

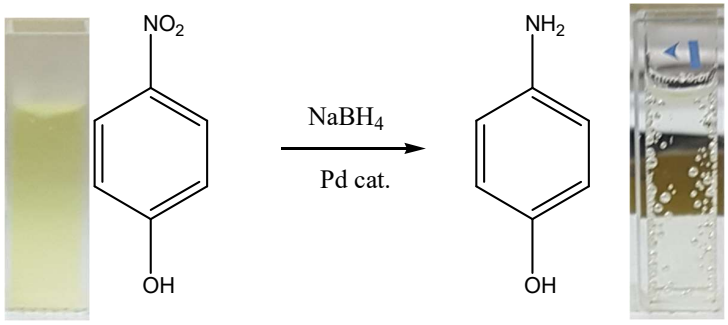

The catalytic hydrogenation of 4-NP to 4-AP (E_0 = -1.76 V) by $NaBH_4$ is thermodynamically feasible as it is a very strong reductant (E_0 = -1.33 V), causing the difference between their standard electrode potential to be greater than zero (ΔE_0=+0.67 V). However, the reaction is kinetically restricted and cannot take place without an efficient metal catalyst. Pd NCs overcome the large activation energy barrier between electron donor and electron acceptor species and play a significant role in the transfer of an electron from BH_4^- to 4-NP.

The following Figure 32 shows the absorption spectrum of the 4-NP aqueous solution (0.1mM) that has a typical absorption peak at about 317 nm, whereas at alkaline pH, 4-NP in presence of excess $NaBH_4$ shows a red-shifted characteristic absorption at about 400 nm due to the formation of 4-nitrophenolate ion.[65] Without the addition of nanocatalysts, the solution remained bright yellow and did not show any change of absorbance at 400 nm with time.

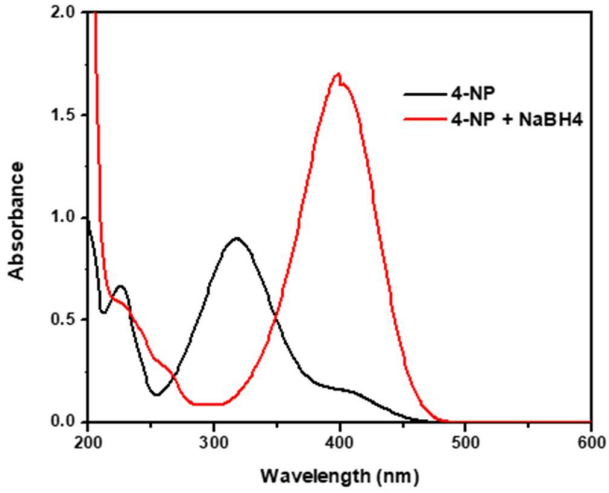

Figure 32. UV-VIS spectra of 4-NP and 4-NP after the addition of $NABH_4$.

If Pd NCs are employed in the reaction system of 4-NP and $NaBH_4$, then the reduction reaction can be initiated rapidly. This reaction may be followed via UV−VIS spectroscopy. The absorption peak at 400 nm gradually decreases in intensity along with a concomitant rise in the absorbance of a new peak at 300 nm, indicating the formation of 4-Aminophenol (4-AP).[65] Correspondingly, Figure 34 displays the time-dependent UV−VIS absorption spectra of 4-NP during its reduction by $NaBH_4$ to 4-AP catalyzed by different sized Pd NCs. The completion of the reaction can be confirmed by the decolorization of the reaction mixture from bright yellow (4-NP) to colourless (4-AP). Also, 4- AP is the only product formed in this reaction which is evident from the occurrence of one isobestic point in the UV-VIS absorption spectra.

Since the concentration of $NaBH_4$ largely exceeded that of 4-NP, the rate of reduction reactions should be first order with respect to the reducing agent. The hydrogenation reaction followed pseudo-first-order rate kinetics, and the apparent rate constant (k_{app}) was determined from the slope of the linear regression of ln (A_t/A_0) versus reaction time. In the below Figure 33, the linear relationships can be found for the Pd NCs synthesized in 0%, 25%, 50%, 75%, and 100% (v/v) EG in water respectively.

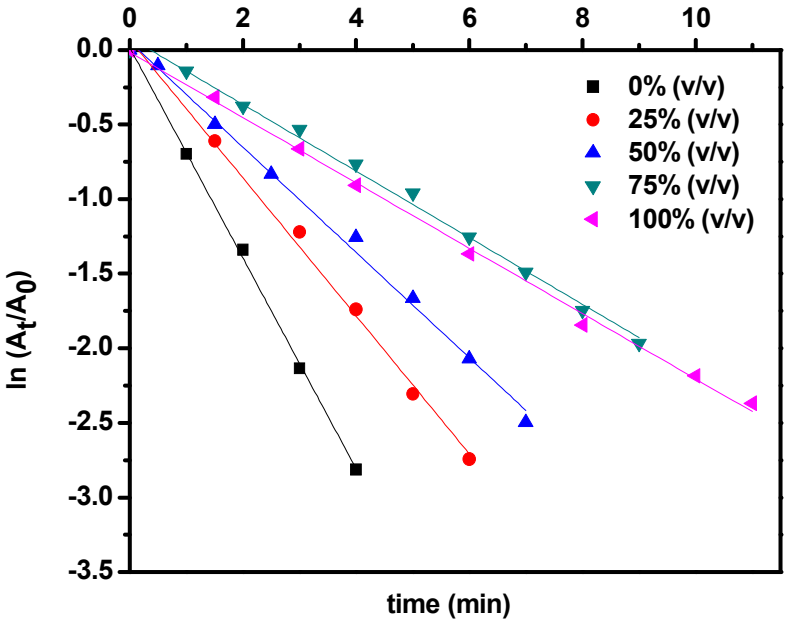

Figure 33. Kinetic study of catalytic reduction reaction of 4-NP (0.1 mM) reduction catalyzed by 10µL of Pd NCs (0.4 mg/mL) synthesized in 0 %, 25 %, 50 %, 75 % and 100 % (v/v) of EG in water.

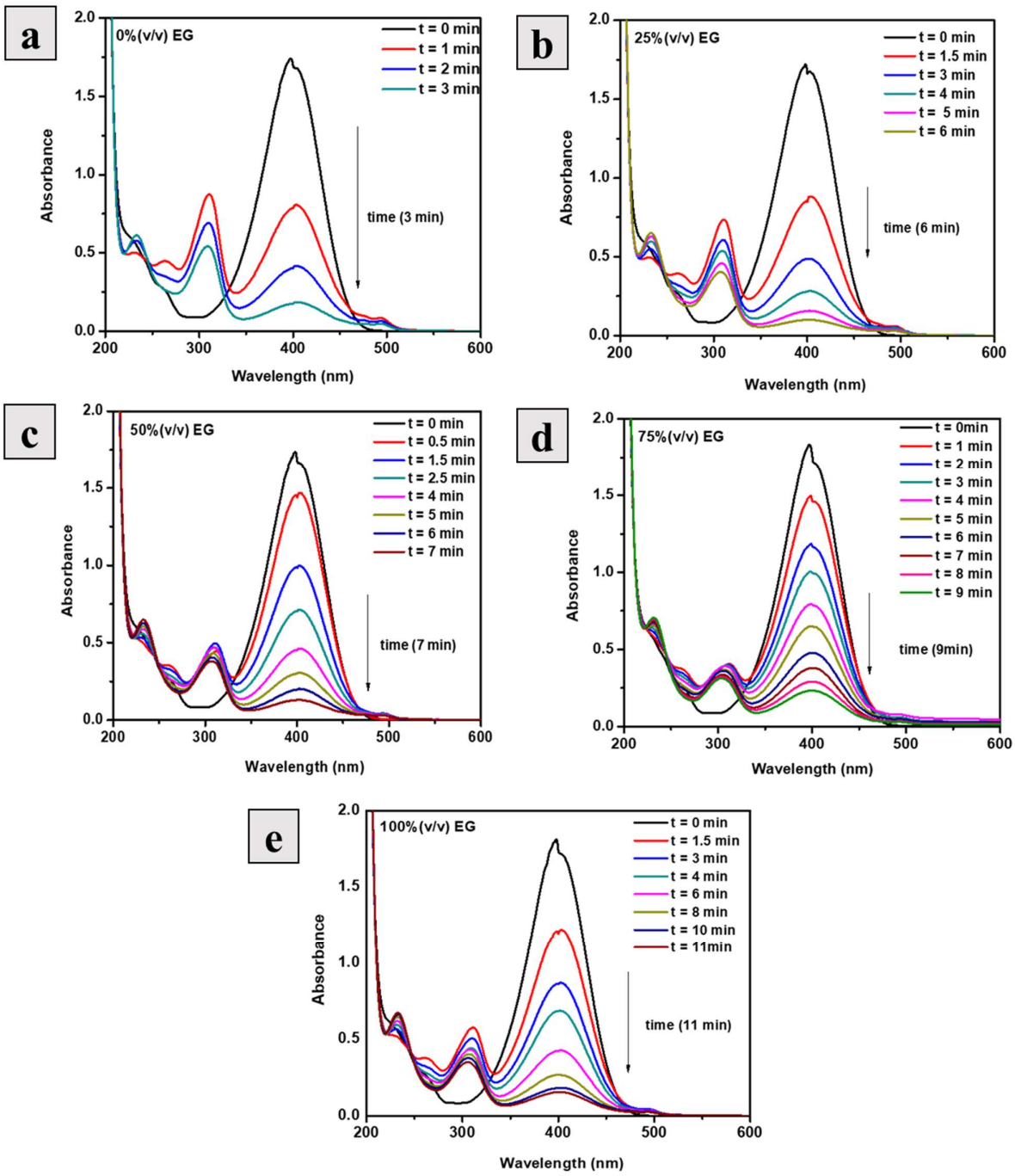

Figure 34. Absorption spectra of the solution of 4-NP (0.1 mM) during its reduction by $NaBH_4$ to 4-AP as a function of time catalyzed by Pd NCs in a) 0 % b) 25 % c) 50 % d)75 % e)100 % (v/v) of EG in water.

B. 2-hydroxy- 5-nitrobenzaldehyde

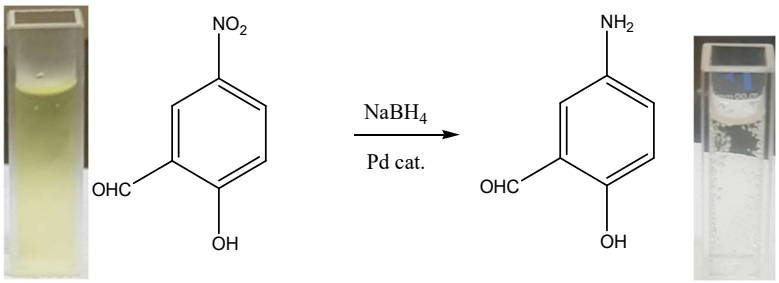

Figure 34 shows the plot of ln (A_t/A_0) versus reaction time for the conversion of 2-hydroxy-5-nitrobenzaldehyde (2,5-NB) to 5-Amino-2-hydroxybenzaldehyde (5,2-AB). The following Figure 35 shows the UV-VIS absorption study. We observe a decrease in intensity of peak at 400 nm along with the concomitant rise of the peak at 300 nm. For 10µL of PdNCs synthesized in 0 %, 25 %, 50 %, 75 %, and 100 %(v/v) of EG in water, it took approximately 5 min, 10 min, 30 min, 45 min, and 60 min respectively for complete conversion. It is observed that the reduction of 2,5-NB does not start immediately after the mixing of reactants and catalyst in the case of Pd NCs synthesized in 75 % and 100 % (v/v) of EG in water. Induction time can be due to the presence of oxide layer over the Pd NCs surface or different rate of diffusion of reactant molecules into the polymeric network to access Pd NPs surface.[81]

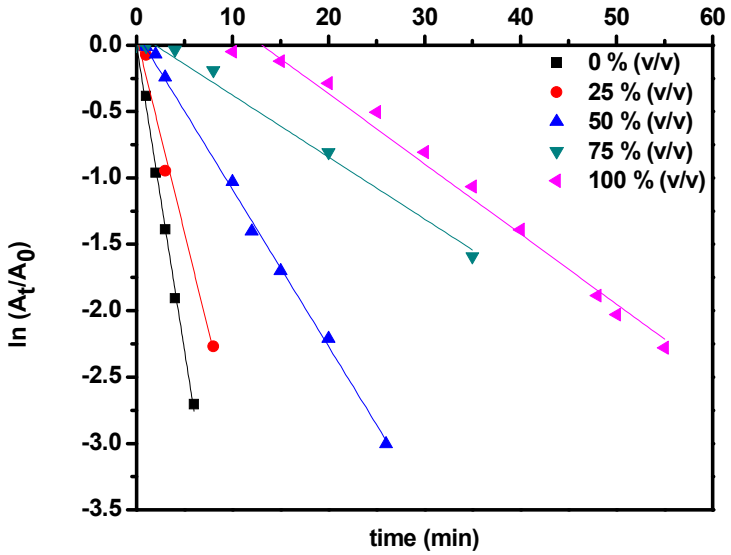

Figure 35. Kinetic study of catalytic reduction reaction of 2,5-NB (0.1 mM) catalyzed by 10µL of Pd NCs (0.4 mg/mL) synthesized in 0 %, 25 %, 50 %, 75 % and 100 % (v/v) of EG in water.

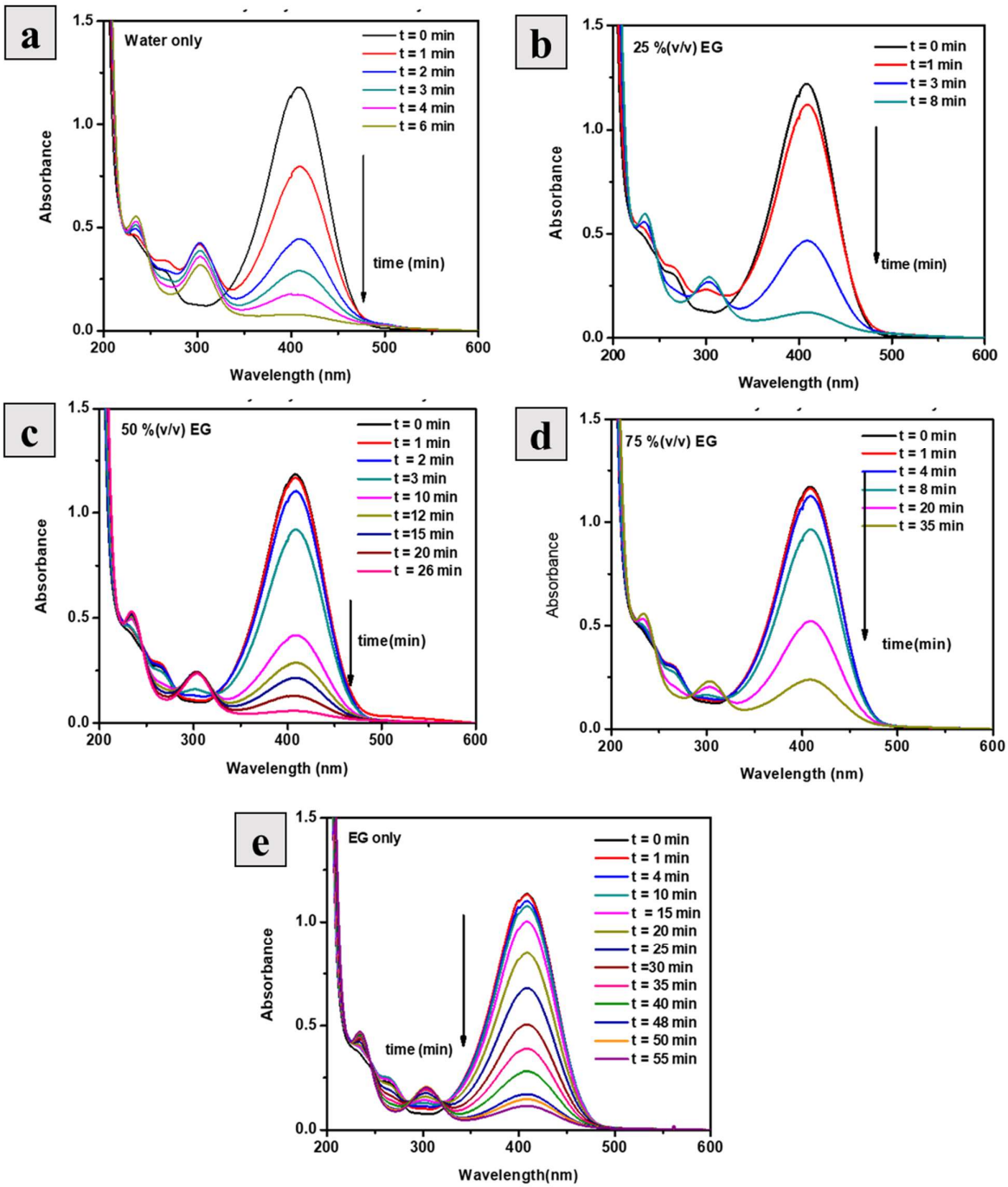

Figure 36. Absorption spectra of the solution of 2,5-NB (0.1 mM) during its reduction by $NaBH_4$ to 5,2-AB as a function of time catalyzed by Pd NCs synthesized in a) 0% b) 25% c) 50% d)75% e)100% (v/v) of EG in water.

C. 2-Nitrophenol

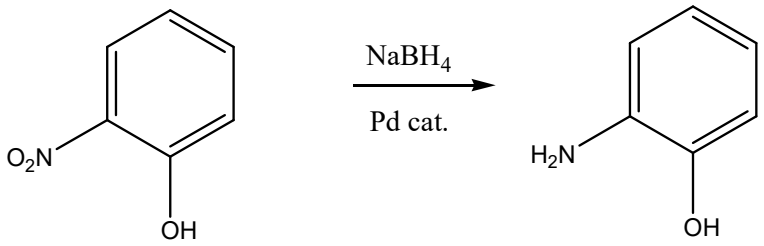

The catalytic reduction of 2-Nitrophenol (2-NP) reduction to 2-Aminophenol (2-AP) follows pseudo-first-order kinetics as observed in Figure 36. Figure 37 shows the UV absorption spectra for 2-NP reduction to 2-AP with the different Pd NCs. The progress was easily monitored by recording the decrease in absorbance of the reaction mixture at 420 nm with time, after the addition of the catalyst. A new peak emerges around 300 nm corresponding to 2-AP and progressively increases in intensity over time.[82] Here again, Pd NCs showed the best catalytic performance for 2-NP reduction taking about 20 min to complete reaction, while for PdNCs synthesized in EG, it takes much longer time > 1hr.

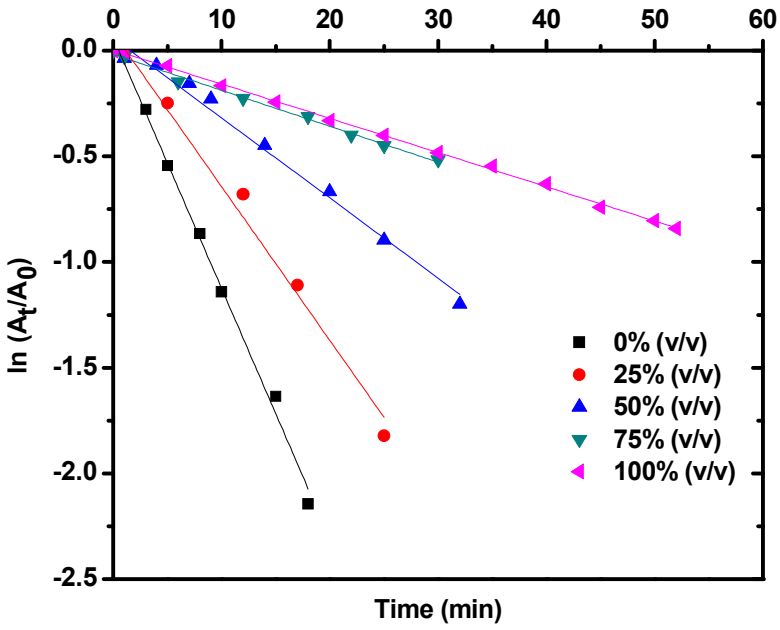

Figure 37. Kinetic study of catalytic reduction reaction of 2-NP (0.5 mM) catalyzed by 9µl of Pd NCs (0.4 mg/mL) synthesized in 0 %, 25 %, 50 %, 75 % and 100 % (v/v) of EG in water

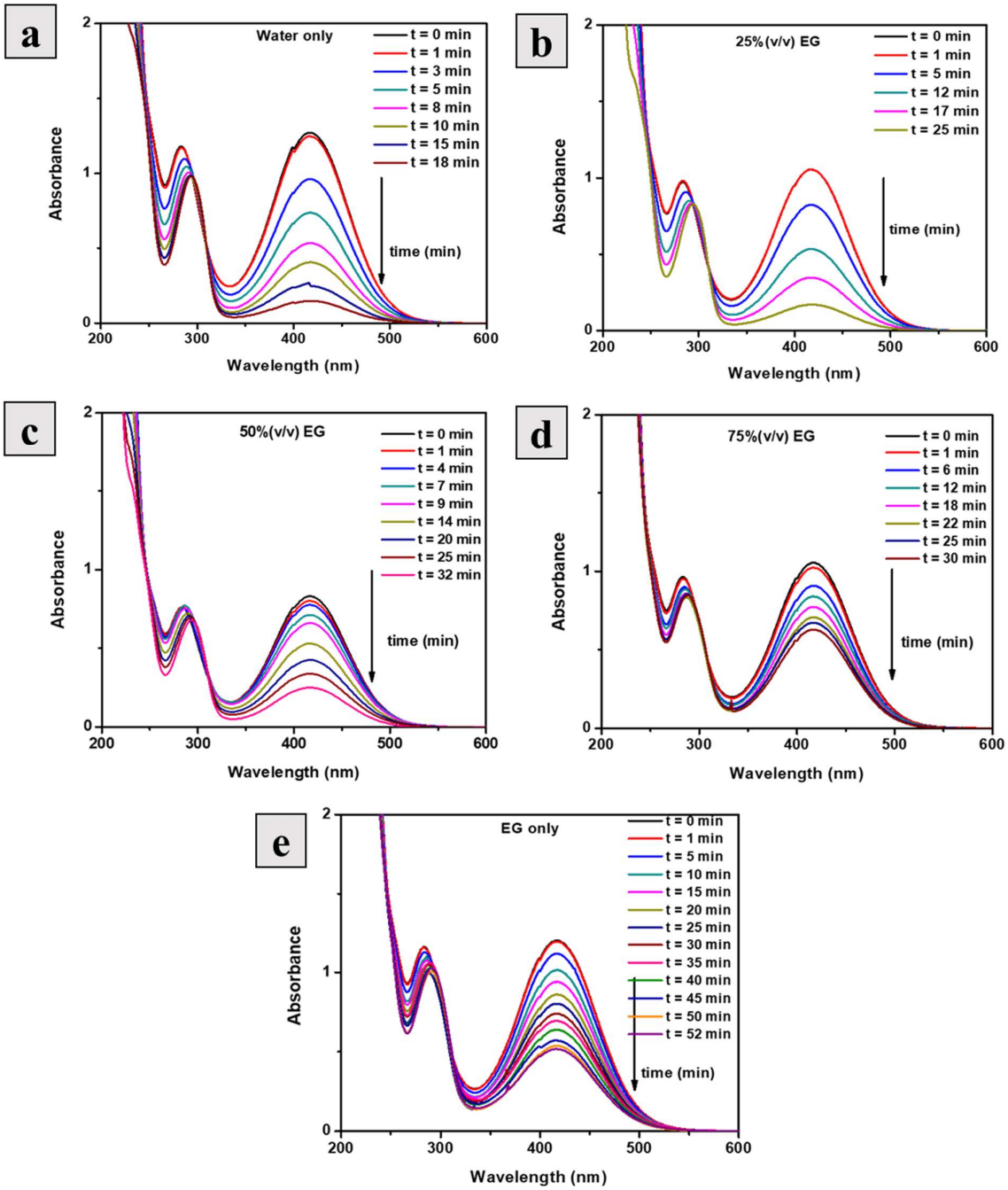

Figure 38. Absorption spectra of the solution of 2-NP (0.5 mM) during its reduction by $NaBH_4$ to 2-AP as a function of time catalyzed by Pd NCs synthesized in a) 0% b) 25% c) 50% d)75% e)100% (v/v) of EG in water.

D. 3-Nitrophenol

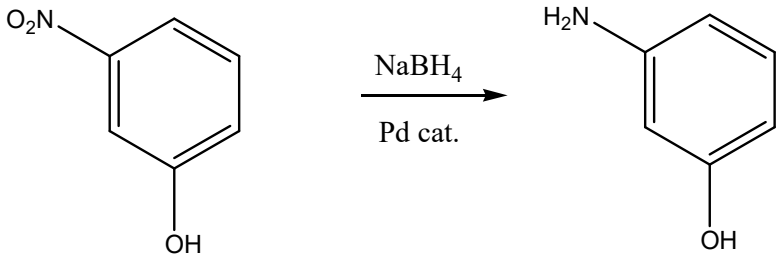

Plots of ln (C_t/C_o) vs time (minutes) for reduction of 3-Nitrophenol (3-NP) to 3-Aminophenol (3-NA) catalyzed by Pd NCs synthesized in different solvent mixtures of H_2O-EG are shown in Figure 38. A similar trend is observed in the time taken for completion of reaction with Pd NCs synthesized in water as the most efficient. The UV-VIS absorption spectra for the catalytic reduction of 3-NP to 3-AP is shown in Figure 39. We could observe the reaction progress by the disappearance of the absorption peak around 390 nm over time corresponding to phenolate ions and the emergence of a new peak around 290 nm corresponding to 3-NA product.[82]

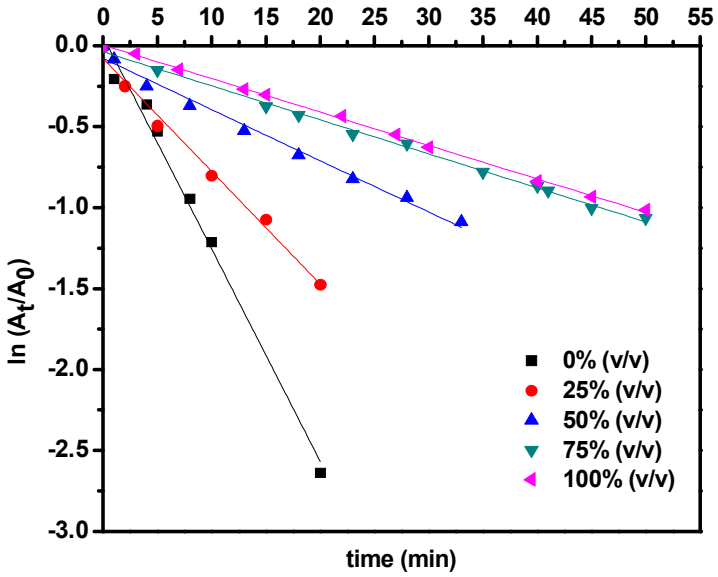

Figure 38. Kinetic study of catalytic reduction reaction of 3-NP (0.5 mM) catalyzed by 9µl of Pd NCs (0.4 mg/mL) synthesized in 0 %, 25 %, 50 %, 75 % and 100 % (v/v) of EG in water

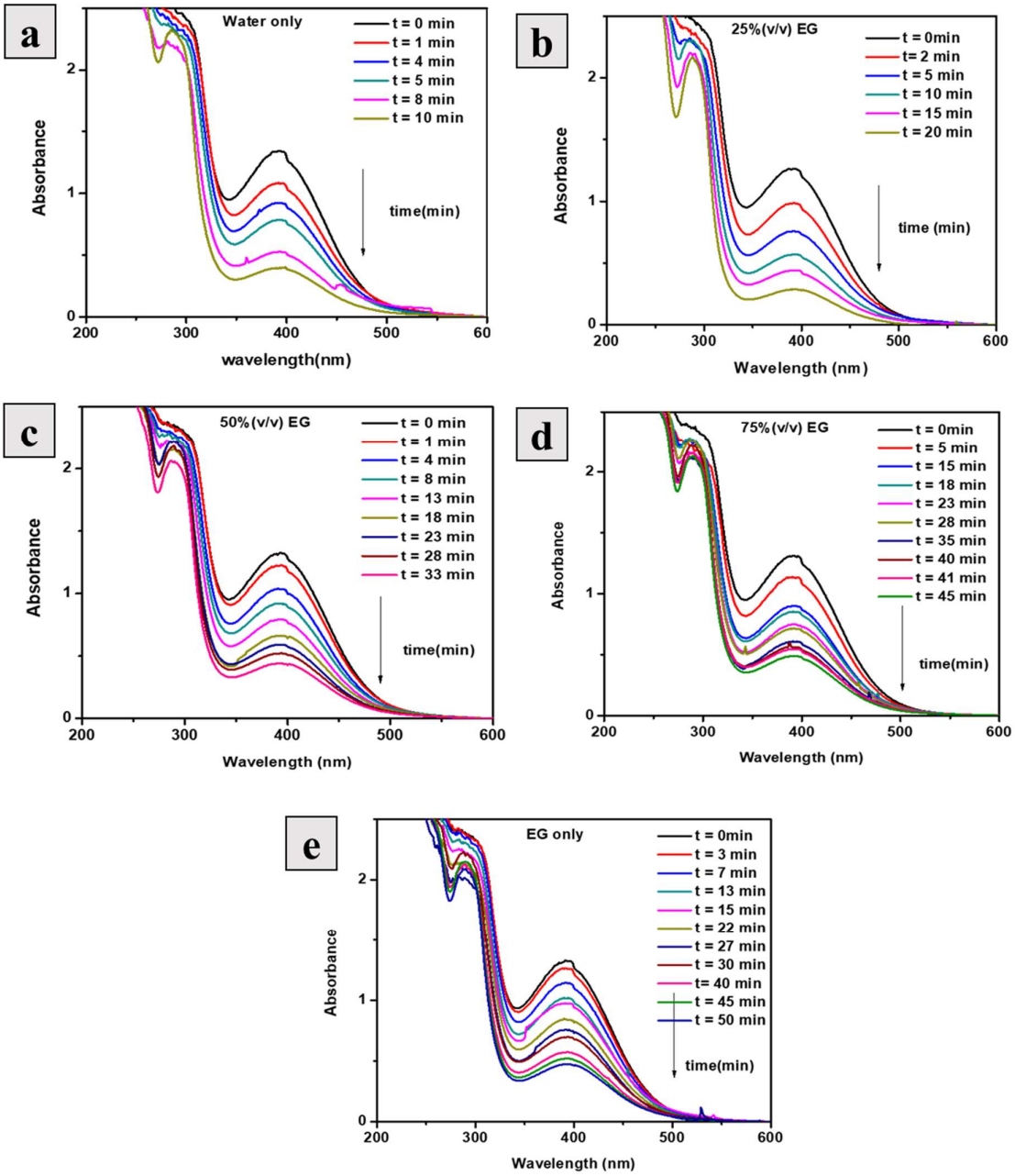

Figure 39. Absorption spectra of the solution of 3-NP during its reduction by $NaBH_4$ to 3-AP as a function of time catalyzed by Pd NCs synthesized in a) 0% b) 25% c) 50% d)75% e)100% (v/v) of EG in water.

E. 4-Nitroaniline

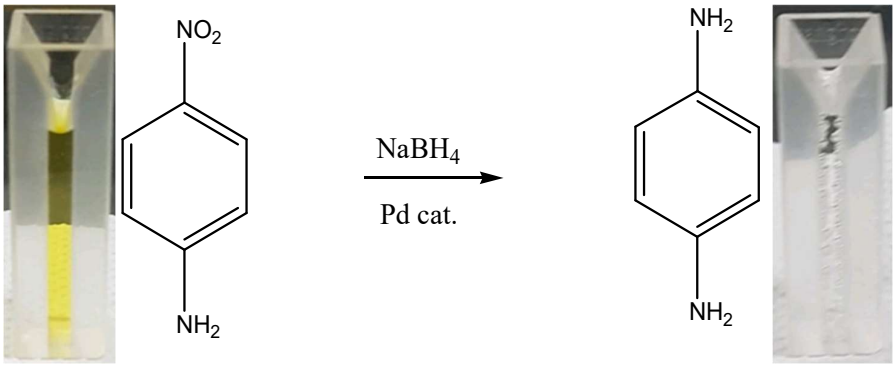

A linear correlation is observed between ln (C_t/C_0) and time, obtaining the rate constant from the slope of the graph, as depicted in Figure 40. The UV-VIS absorption spectra for the catalytic reduction of 4-Nitroaniline (4-NA) to p-phenylenediamine (4-AA) is shown in Figure 41. The peak at 375nm was found to be gradually decreasing over time. At the same time, two new peaks were observed at 240 nm and 310 nm which correspond to 4-AA .[81] Reaction mixture turned from bright yellow to colourless indicating the completion of the reaction. The reduction was completed in 10 minutes by Pd NCs synthesized in water, however, it took about 50 minutes for Pd NCs synthesized in EG.

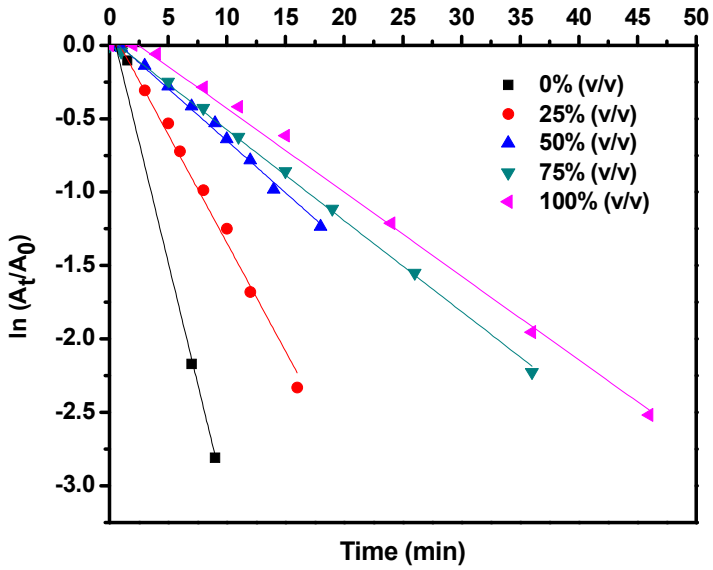

Figure 40. Kinetic study of catalytic reduction reaction of 4-NA (0.2 mM) catalyzed by 6µl of Pd NCs (0.4 mg/mL) synthesized in 0 %, 25 %, 50 %, 75 % and 100 % (v/v) of EG in water

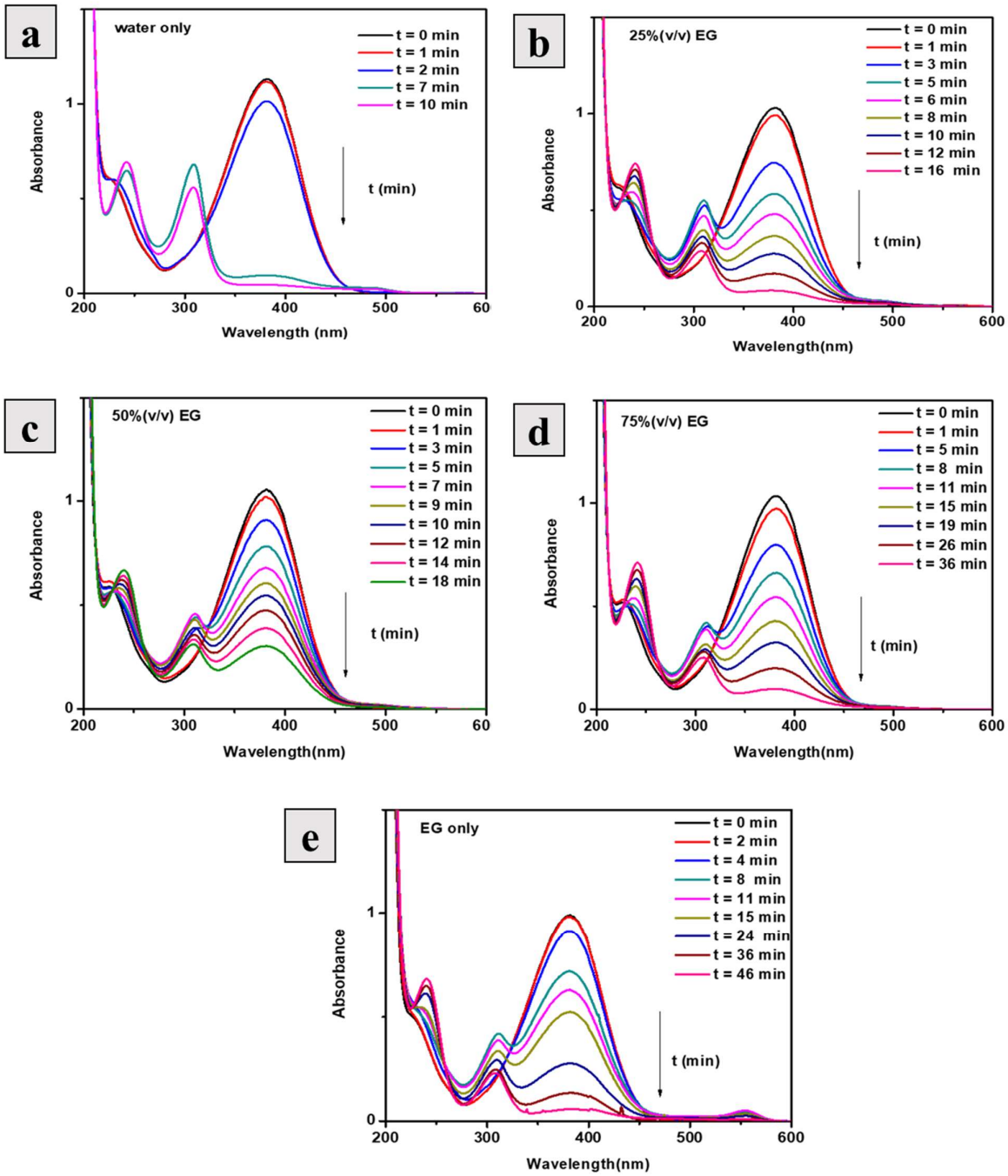

Figure 41. Absorption spectra of the solution of 4-NA during its reduction by $NaBH_4$ to 4-AA as a function of time catalyzed by Pd NCs synthesized in a) 0% b) 25% c) 50% d)75% e)100% (v/v) of EG in water.

3.4 Electrochemical impedance measurements for PdNCs

The Nyquist plots in Figure 42 demonstrated a semi-circle and a Warburg diffusion line which is an indication that the electrochemical process on the electrode surface is kinetically controlled at higher frequencies and diffusion controlled at lower frequencies. We observe that Nyquist plots are dominated by the linear region, which indicates that the electron transfer occurring on the electrode surface is heavily influenced by a diffusion-limited process between the bulk solution and the electrode surface

The charge transfer resistance is a measure of the resistance associated with the electron transfer process. A low R_{ct} indicates a facile interfacial electron transfer process. The results (Table 10) revealed that the PdNCs have comparable charge transfer resistance (R_{ct}) values in the range 100 to 110Ω . This suggests that they have similar electron transfer kinetics. These values are also dependent on ionic concentrations, oxide layers, electrode area, surface roughness, impurity adsorption, etc. Despite similar charge transfer resistance, Pd NCs showed very different catalytic activity. It suggests that in case of Pd NCs synthesized in water, active sites for facile adsorption of reactant molecules are relatively more available.

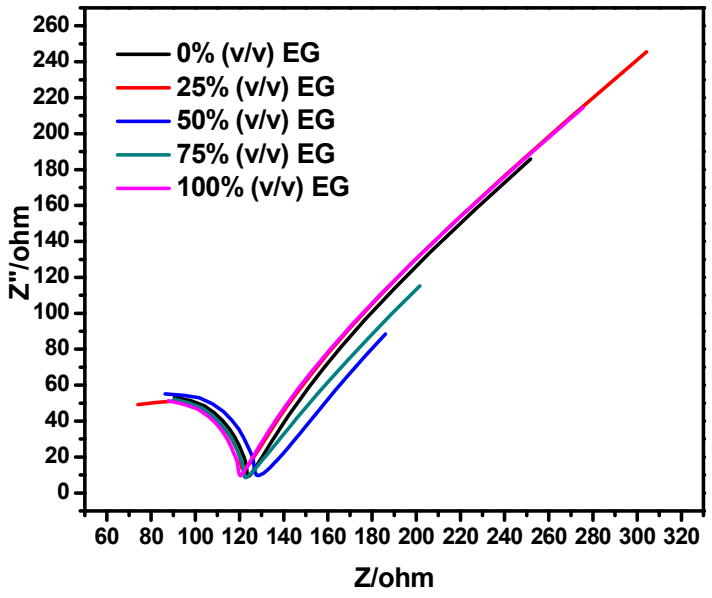

Figure 42. Nyquist plots for Pd NCs synthesized in a) 0% b) 25% c) 50% d)75% e)100% (v/v) of EG in water.

Table 10. Charge transfer resistances for 1mg PdNCs synthesized in a) 0% b) 25% c) 50% d)75% e)100% (v/v) of EG in water.

Sample	%(v/v) EG in water	Rct(Ω)
S1	0%	108.9±5.3
S2	25%	107.1±7.8
S3	50%	108.7±1.0
S4	75%	103.2±1.2
S5	100%	104.1±3.7

4. Conclusions

In conclusions, to understand role of solvent in synthesis and subsequent catalytic activity, we have carried out solvothermal synthesis of Pd NCs. Herein, quasi-spherical palladium nanoparticles were prepared by reducing palladium salt precursor H_2PdCl_4 in mixture of two common solvents water and ethylene glycol with significantly different viscosity and dipole moment, in the presence of PVP at 200°C for 12 h. The influence of solvent composition in monitoring the average diameter and the nature of surface of palladium nanoparticles has been examined by keeping all other reaction conditions (precursor concentration, temperature, time and pH) identical. The systematic increase in the fraction of EG : 0%(v/v) , 25%(v/v) , 50%(v/v) , 75% (v/v) ,100%(v/v) in the mixture of H_2O-EG led to corresponding increase of the Pd NCs size from 6.4 nm, 7.9 nm, 9.8 nm, 12.1 nm to 16.9 nm respectively . The differences in size of PdNCs can be attributed to the intrinsic properties of solvent such as viscosity, boiling point and dielectric constant influencing nucleation and growth rate of the nanoparticles. Furthermore, catalytic properties of the Pd NCs synthesized from these solvents have been investigated to understand how appropriate solvent of synthesis can improve efficiency of the catalyst nanoparticles. Pd NCs synthesised in water showed far superior efficiency towards Suzuki-Miyuara coupling and catalytic reduction of nitroaromatics as compared to that of synthesized in 100% (v/v) EG. The turnover frequencies normalized by fraction of surface atoms (s-TOF) for Suzuki-Miyuara coupling, though expected to be approximately same, was found to decrease significantly by factor of 10 as the solvent of synthesis is varied from water to ethylene glycol. Similarly, kinetic rate constants observed were not found to be entirely consistent with size of Pd NCs. The substantial disparity in catalytic properties has been rationalized in terms of different nature of catalytic surface owing to different solvent of synthesis. This study illustrates the complexity of the real -world nanocatalysts where their catalytic activity is also dependent on the solvent of their synthesis.

5. Scope of the work

The study highlights that for obtaining desired nanocatalysts, optimizing of the solvent of synthesis is crucial. It is indicated that the solvent of synthesis not only tune the size of nanocatalyst but also can cause modifications in the surface properties. While the methods used in this study cannot provide detailed information on the surface properties of the PdNCs, the different catalytic performance observed for PdNCs synthesized in water, ethylene glycol and solvent mixtures have suggested hidden role of the solvent of synthesis in determining the catalytic efficiency of the nanoparticles.

For a better understanding of the surface, it is imperative to study different contributions (electronic and geometric). Besides the influence of the size and shape of nanocatalysts, the chemical and geometric heterogeneities at the interface also determine their eventual catalytic performance. It is a challenge to isolate the effect of solvent alone from other factors (nanoparticle structure, support, etc.) A characterization technique, able to distinguish the role of solvent in passivation of catalyst, is needed. For example, XPS studies can reveal whether oxide layer formation at the surface is dependent on the solvent. We can extend the study to compare the electrocatalytic performance of the catalysts. It can help in interpreting the diffusion rate of reactants towards catalyst surface, which would unveil geometric abnormalities due to surface defects, capping agents, etc. The comprehensive study of the parameters involved in synthesis would allow the prediction of properties of the nanocatalysts.

Bibliography

(1) Wu, Y.; Wang, D.; Li, Y. Understanding of the Major Reactions in Solution Synthesis of Functional Nanomaterials. *Sci. China Mater.* **2016**, *59* (11), 938–996. https://doi.org/10.1007/s40843-016-5112-0.

(2) Xia, Y.; Xiong, Y.; Lim, B.; Skrabalak, S. E. Shape-Controlled Synthesis of Metal Nanocrystals: Simple Chemistry Meets Complex Physics? *Angew. Chemie - Int. Ed.* **2009**, *48* (1), 60–103. https://doi.org/10.1002/anie.200802248.

(3) Iqbal, M.; Kaneti, Y. V.; Kim, J.; Yuliarto, B.; Kang, Y. M.; Bando, Y.; Sugahara, Y.; Yamauchi, Y. Chemical Design of Palladium-Based Nanoarchitectures for Catalytic Applications. *Small* **2019**, *15* (6), 1–27. https://doi.org/10.1002/smll.201804378.

(4) Cao, S.; Tao, F. F.; Tang, Y.; Li, Y.; Yu, J. Size- and Shape-Dependent Catalytic Performances of Oxidation and Reduction Reactions on Nanocatalysts. *Chem. Soc. Rev.* **2016**, *45* (17), 4747–4765. https://doi.org/10.1039/c6cs00094k.

(5) Han, N.; Cao, S.; Han, J.; Hu, Y.; Zhang, X.; Guo, R. Surface Cavities of Ni(OH)2 Nanowires Can Host Au Nanoparticles as Supported Catalysts with High Catalytic Activity and Stability. *J. Mater. Chem. A* **2016**, *4* (7), 2590–2596. https://doi.org/10.1039/c5ta10258h.

(6) Salamon, A. W.; Courtney, P.; Shuttler, I. Nanotechnology and Engineered Nanomaterials. 2010.

(7) Rodrigues, T. S.; Da Silva, A. G. M.; Camargo, P. H. C. Nanocatalysis by Noble Metal Nanoparticles: Controlled Synthesis for the Optimization and Understanding of Activities. *J. Mater. Chem. A* **2019**, *7* (11), 5857–5874. https://doi.org/10.1039/c9ta00074g.

(8) Heuer-Jungemann, A.; Feliu, N.; Bakaimi, I.; Hamaly, M.; Alkilany, A.; Chakraborty, I.; Masood, A.; Casula, M. F.; Kostopoulou, A.; Oh, E.; Susumu, K.; Stewart, M. H.; Medintz, I. L.; Stratakis, E.; Parak, W. J.; Kanaras, A. G. The Role of Ligands in the Chemical Synthesis and Applications of Inorganic Nanoparticles. *Chem. Rev.* **2019**, *119* (8), 4819–4880. https://doi.org/10.1021/acs.chemrev.8b00733.

(9) Seisenbaeva, G. A.; Kessler, V. G. Precursor Directed Synthesis - “Molecular” Mechanisms in the Soft Chemistry Approaches and Their Use for Template-Free Synthesis of Metal, Metal Oxide and Metal Chalcogenide Nanoparticles and Nanostructures. *Nanoscale* **2014**, *6* (12), 6229–6244. https://doi.org/10.1039/c3nr06336d.

(10) López, R.; Vigueras-Santiago, E.; Acuña-Avila, P. E.; Hernández-López, S.; López-Téllez, G.; Zaragoza-Contreras, E. A.; Hernández-Escobar, C. A.; Antünez, W.; Torres-Gómez, N. Role of the Vacuum Pressure and Temperature in the Shape of Metal Zn Nanoparticles. *Bull. Mater. Sci.* **2015**, *38* (7), 1777–1781. https://doi.org/10.1007/s12034-015-1048-z.

(11) Nikam, A. V.; Prasad, B. L. V.; Kulkarni, A. A. Wet Chemical Synthesis of Metal Oxide Nanoparticles: A Review. *CrystEngComm* **2018**, *20* (35), 5091–5107. https://doi.org/10.1039/C8CE00487K.

(12) Jimenez-Ruiz, A.; Perez-Tejeda, P.; Grueso, E.; Castillo, P. M.; Prado-Gotor, R. Nonfunctionalized Gold Nanoparticles: Synthetic Routes and Synthesis Condition Dependence. *Chem. - A Eur. J.* **2015**, *21* (27), 9596–9609. https://doi.org/10.1002/chem.201405117.

(13) Wei, L.; Mao, Y.; Wei, Y.; Li, J.; Nie, X.; Zhao, X.; Fan, Y.; Sun, S. Concentration-Mediated Shape Evolution of Palladium Nanocrystals and Their Structure-Electrocatalytic Functionality. *Cryst. Growth Des.* **2019**, *19*, 1532–1539. https://doi.org/10.1021/acs.cgd.8b00892.

(14) Daruich De Souza, C.; Ribeiro Nogueira, B.; Rostelato, M. E. C. M. Review of the Methodologies Used in the Synthesis Gold Nanoparticles by Chemical Reduction. *J. Alloys Compd.* **2019**, *798*, 714–740. https://doi.org/10.1016/j.jallcom.2019.05.153.

(15) Sharifi Dehsari, H.; Halda Ribeiro, A.; Ersöz, B.; Tremel, W.; Jakob, G.; Asadi, K. Effect of Precursor Concentration on Size Evolution of Iron Oxide Nanoparticles. *CrystEngComm* **2017**, *19* (44), 6694–6702. https://doi.org/10.1039/c7ce01406f.

(16) Koczkur, K. M.; Mourdikoudis, S.; Polavarapu, L.; Skrabalak, S. E. Polyvinylpyrrolidone (PVP) in Nanoparticle Synthesis. *Dalt. Trans.* **2015**, *44* (41), 17883–17905. https://doi.org/10.1039/c5dt02964c.

(17) Wiley, B. J.; Xiong, Y. Oxidative Etching for Controlled Synthesis of Metal Nanocrystals: Atomic Addition and Subtraction. *Chem. Soc. Rev.* **2014**, *43* (17), 6177–6474. https://doi.org/10.1039/c4cs00136b.

(18) Soltani, N.; Saion, E.; Erfani, M.; Rezaee, K.; Bahmanrokh, G.; Drummen, G. P. C.; Bahrami, A.; Hussein, M. Z. Influence of the Polyvinyl Pyrrolidone Concentration on Particle Size and Dispersion of ZnS Nanoparticles Synthesized by Microwave Irradiation. *Int. J. Mol. Sci.* **2012**, *13* (10), 12412–12427. https://doi.org/10.3390/ijms131012412.

(19) Mostafa, S.; Behafarid, F.; Croy, J. R.; Ono, L. K.; Li, L.; Yang, J. C.; Frenkel, A. I.; Cuenya, B. R. Shape-Dependent Catalytic Properties of Pt Nanoparticles. *J. Am. Chem. Soc.* **2010**, *132* (44), 15714–15719. https://doi.org/10.1021/ja106679z.

(20) Costanzo, S.; Simon, G.; Richardi, J.; Colomban, P.; Lisiecki, I. Solvent Effects on Cobalt Nanocrystal Synthesis - A Facile Strategy to Control the Size of Co Nanocrystals. *J. Phys. Chem. C* **2016**, *120* (38), 22054–22061. https://doi.org/10.1021/acs.jpcc.6b07293.

(21) Maharaz, M. N.; Halimah, M. K.; Paiman, S.; Saiden, N. M.; Alibe, I. M. Influence of Solvents and Irradiation Time on Structural and Optical Properties of Cubic PbS Nanoparticles. *Int. J. Electrochem. Sci.* **2018**, *13* (10), 9317–9332. https://doi.org/10.20964/2018.10.37.

(22) Farrukh, M. A.; Muneer, I.; Butt, K. M.; Batool, S.; Fakhar, N. Effect of Dielectric Constant of Solvents on the Particle Size and Bandgap of La/SnO2-TiO2 Nanoparticles and Their Catalytic Properties. *J. Chinese Chem. Soc.* **2016**, *63* (12), 952–959. https://doi.org/10.1002/jccs.201600205.

(23) Jiao, M.; Jing, L.; Liu, C.; Hou, Y.; Huang, J.; Wei, X.; Gao, M. Differently Sized Magnetic/Upconversion Luminescent NaGdF4:Yb,Er Nanocrystals: Flow Synthesis and Solvent Effects. *Chem. Commun.* **2016**, *52* (34), 5872–5875. https://doi.org/10.1039/c6cc01686c.

(24) Wiranwetchayan, O.; Promnopas, S.; Thongtem, T.; Chaipanich, A.; Thongtem, S. Effect of Alcohol Solvents on TiO2 Films Prepared by Sol–Gel Method. *Surf. Coatings Technol.* **2017**, *326*, 310–315. https://doi.org/10.1016/j.surfcoat.2017.07.068.

(25) Zhang, Y.; Wang, J.; Wang, W.; Zhao, F.; Xu, K. Solvent Effect on Structure, Morphology and Catalytic Activity on Ammonium Perchlorate of Nano-MgWO4. *Nano* **2019**. https://doi.org/10.1142/S1793292019501352.

(26) Bernard, A.; Zhang, K.; Larson, D.; Tabatabaei, K.; Kauzlarich, S. M. Solvent Effects on Growth, Crystallinity, and Surface Bonding of Ge Nanoparticles. *Inorg. Chem.* **2018**, *57* (9), 5299–5306. https://doi.org/10.1021/acs.inorgchem.8b00334.

(27) Šarić, A.; Despotović, I.; Štefanić, G. Alcoholic Solvent Influence on ZnO Synthesis: A Joint Experimental and Theoretical Study. *J. Phys. Chem. C* **2019**, *123* (48), 29394–29407. https://doi.org/10.1021/acs.jpcc.9b07411.

(28) Song, J.; Kim, D.; Lee, D. Size Control in the Synthesis of 1-6 Nm Gold Nanoparticles via Solvent-Controlled Nucleation. *Langmuir* **2011**, *27* (22), 13854–13860. https://doi.org/10.1021/la203113r.

(29) Sharma, R.; Wang, Y.; Li, F.; Chamier, J.; Andersen, S. M. Particle Size-Controlled Growth of Carbon-Supported Platinum Nanoparticles (Pt/C) through Water-Assisted Polyol Synthesis. *ACS Omega* **2019**, *4* (13), 15711–15720. https://doi.org/10.1021/acsomega.9b02351.

(30) Jiang, Y.; Wu, X.-J.; Li, Q.; Li, J.; Xu, D. Facile Synthesis of Gold Nanoflowers with High Surface-Enhanced Raman Scattering Activity. *Nanotechnology* **2011**, *22* (38), 385601. https://doi.org/10.1088/0957-4484/22/38/385601.

(31) Thakur, P.; Joshi, S. S. Effect of Alcohol and Alcohol/Water Mixtures on Crystalline Structure of CdS Nanoparticles. *J. Exp. Nanosci.* **2012**, *7* (5), 547–558. https://doi.org/10.1080/17458080.2010.543990.

(32) Trushina, D. B.; Bukreeva, T. V.; Antipina, M. N. Size-Controlled Synthesis of Vaterite Calcium Carbonate by the Mixing Method: Aiming for Nanosized Particles. *Cryst. Growth Des.* **2016**, *16* (3), 1311–1319. https://doi.org/10.1021/acs.cgd.5b01422.

(33) Huang, Y.; Liao, J.; Liu, C.; Lu, T.; Xing, W. The Size-Controlled Synthesis of Pd / C Catalysts by Different Solvents for Formic Acid Electrooxidation. *Nanotechnology* **2009**, 105604. https://doi.org/10.1088/0957-4484/20/10/105604.

(34) Uekawa, N.; Kitamura, M.; Ishii, S.; Kojima, T.; Kakegawa, K. Low-Temperature

Synthesis of ZnO Nanoparticles by Heating of Zn(OH) 2 in a Neutral Mixed Solution of Ethanol and H2O. *Journal of the Ceramic Society of Japan*. Journal of the Ceramic Society of Japan 2005, pp 439–441. https://doi.org/10.2109/jcersj.113.439.

(35) Roca, R. A.; Leite, E. R. Size and Shape Tailoring of Titania Nanoparticles Synthesized by Solvothermal Route in Different Solvents. *J. Am. Ceram. Soc.* **2013**, *96* (1), 96–102. https://doi.org/10.1111/jace.12078.

(36) Douglas, F. J.; MacLaren, D. A.; Murrie, M. A Study of the Role of the Solvent during Magnetite Nanoparticle Synthesis: Tuning Size, Shape and Self-Assembly. *RSC Adv.* **2012**, *2* (21), 8027–8035. https://doi.org/10.1039/c2ra20494k.

(37) Xu, L.; Hu, Y. L.; Pelligra, C.; Chen, C. H.; Jin, L.; Huang, H.; Sithambaram, S.; Aindow, M.; Joesten, R.; Suib, S. L. ZnO with Different Morphologies Synthesized by Solvothermal Methods for Enhanced Photocatalytic Activity. *Chem. Mater.* **2009**, *21* (13), 2875–2885. https://doi.org/10.1021/cm900608d.

(38) Semlali, S.; Cormary, B.; De Marco, M. L.; Majimel, J.; Saquet, A.; Coppel, Y.; Gonidec, M.; Rosa, P.; Drisko, G. L. Effect of Solvent on Silicon Nanoparticle Formation and Size: A Mechanistic Study. *Nanoscale* **2019**, *11* (11), 4696–4700. https://doi.org/10.1039/c9nr00619b.

(39) Xiong, Y.; Xia, Y. Shape-Controlled Synthesis of Metal Nanostructures: The Case of Palladium. *Adv. Mater.* **2007**, *19* (20), 3385–3391. https://doi.org/10.1002/adma.200701301.

(40) Wang, F.; Hao, G.; Guo, Y.; Ma, X.; Yang, L. Solvent Effects on Preparation of Pd-Based Catalysts: Influence on Properties of Palladium and Its Catalytic Activity for Benzyl Alcohol Oxidation. *Open J. Met.* **2017**, *07* (04), 59–68. https://doi.org/10.4236/ojmetal.2017.74005.

(41) Gu, Yajie; Sun, Shengrui; Liu, Yangqiao; Dong, Manjiang; Yang, Q. Solvent Effect on the Solvothermal Synthesis of Mesoporous NiO Catalysts for Activation of Peroxymonosulfate to Degrade Organic Dyes. *ACS Omega* **2019**, *4*, 17672–17683.

(42) Chowdhury, S. R.; Roy, P. S.; Bhattacharya, S. K. Green Synthesis and Characterization of Polyvinyl Alcohol Stabilized Palladium Nanoparticles: Effect of Solvent on Diameter and Catalytic Activity. *Adv. Nat. Sci. Nanosci. Nanotechnol.*

2017, *8* (2), aa690e. https://doi.org/10.1088/2043-6254/aa690e.

(43) Thongam, D. D.; Gupta, J.; Sahu, N. K.; Bahadur, D. Investigating the Role of Different Reducing Agents, Molar Ratios, and Synthesis Medium over the Formation of ZnO Nanostructures and Their Photo-Catalytic Activity. *J. Mater. Sci.* **2018**, *53* (2), 1110–1122. https://doi.org/10.1007/s10853-017-1587-3.

(44) Sreedhala, S.; Sudheeshkumar, V.; Vinod, C. P. Structure Sensitive Chemical Reactivity by Palladium Concave Nanocubes and Nanoflowers Synthesised by a Seed Mediated Procedure in Aqueous Medium. *Nanoscale* **2014**, *6* (13), 7496–7502. https://doi.org/10.1039/c4nr01283f.

(45) Escaño, M. C. S.; Arevalo, R. L.; Gyenge, E.; Kasai, H. First-Principles Study of Borohydride Adsorption Properties on Osmium Nanoparticles and Surfaces: Understanding the Effects of Facets, Size and Local Sites. *Catal. Sci. Technol.* **2014**, *4* (5), 1301–1312. https://doi.org/10.1039/c3cy01048a.

(46) Campisi, S.; Schiavoni, M.; Chan-Thaw, C. E.; Villa, A. Untangling the Role of the Capping Agent in Nanocatalysis: Recent Advances and Perspectives. *Catalysts* **2016**, *6* (12), 1–21. https://doi.org/10.3390/catal6120185.

(47) Scanlon, M. D.; Peljo, P.; Méndez, M. A.; Smirnov, E.; Girault, H. H. Charging and Discharging at the Nanoscale: Fermi Level Equilibration of Metallic Nanoparticles. *Chem. Sci.* **2015**, *6* (5), 2705–2720. https://doi.org/10.1039/c5sc00461f.

(48) Niu, Z.; Li, Y. Removal and Utilization of Capping Agents in Nanocatalysis. *Chem. Mater.* **2014**, *26* (1), 72–83. https://doi.org/10.1021/cm4022479.

(49) Baker, L. R.; Kennedy, G.; Krier, J. M.; Van Spronsen, M.; Onorato, R. M.; Somorjai, G. A. The Role of an Organic Cap in Nanoparticle Catalysis: Reversible Restructuring of Carbonaceous Material Controls Catalytic Activity of Platinum Nanoparticles for Ethylene Hydrogenation and Methanol Oxidation. *Catal. Letters* **2012**, *142* (11), 1286–1294. https://doi.org/10.1007/s10562-012-0904-3.

(50) Sadeghmoghaddam, E.; Gu, H.; Shon, Y. S. Pd Nanoparticle-Catalyzed Isomerization vs Hydrogenation of Allyl Alcohol: Solvent-Dependent Regioselectivity. *ACS Catal.* **2012**, *2* (9), 1838–1845. https://doi.org/10.1021/cs300270d.

(51) Rossi, L. M.; Fiorio, J. L.; Garcia, M. A. S.; Ferraz, C. P. The Role and Fate of Capping Ligands in Colloidally Prepared Metal Nanoparticle Catalysts. *Dalt. Trans.* **2018**, *47* (17), 5889–5915. https://doi.org/10.1039/c7dt04728b.

(52) McManus, I.; Daly, H.; Thompson, J. M.; Connor, E.; Hardacre, C.; Wilkinson, S. K.; Sedaie Bonab, N.; Ten Dam, J.; Simmons, M. J. H.; Stitt, E. H.; D'Agostino, C.; McGregor, J.; Gladden, L. F.; Delgado, J. J. Effect of Solvent on the Hydrogenation of 4-Phenyl-2-Butanone over Pt Based Catalysts. *J. Catal.* **2015**, *330*, 344–353. https://doi.org/10.1016/j.jcat.2015.06.008.

(53) Van Hoof, A. J. F.; Hermans, E. A. R.; Van Bavel, A. P.; Friedrich, H.; Hensen, E. J. M. Structure Sensitivity of Silver-Catalyzed Ethylene Epoxidation. *ACS Catal.* **2019**, *9* (11), 9829–9839. https://doi.org/10.1021/acscatal.9b02720.

(54) Silvestre-Albero, J.; Rupprechter, G.; Freund, H. J. From Pd Nanoparticles to Single Crystals: 1,3-Butadiene Hydrogenation on Well-Defined Model Catalysts. *Chem. Commun.* **2006**, No. 1, 80–82. https://doi.org/10.1039/b513030a.

(55) Sherwood, James; Clark, James H.; Fairlamb, ian J.S.; Slattery, J. M. Solvent Effects in Palladium Catalysed Cross-Coupling Reactions. *Green Chem.* **2019**, *21*, 2164–2213. https://doi.org/DOI: 10.1039/c9gc00617f.

(56) Parker, H. L.; Sherwood, J.; Hunt, A. J.; Clark, J. H. Cyclic Carbonates as Green Alternative Solvents for the Heck Reaction. *ACS Sustain. Chem. Eng.* **2014**, *2* (7), 1739–1742. https://doi.org/10.1021/sc5002287.

(57) Heidari, B.; Heravi, M. M.; Nabid, M. R.; Sedghi, R.; Hooshmand, S. E. Novel Palladium Nanoparticles Supported on β-Cyclodextrin@graphene Oxide as Magnetically Recyclable Catalyst for Suzuki–Miyaura Cross-Coupling Reaction with Two Different Approaches in Bio-Based Solvents. *Appl. Organomet. Chem.* **2019**, *33* (1), 1–13. https://doi.org/10.1002/aoc.4632.

(58) Ludwig, J. R.; Schindler, C. S. Catalyst: Sustainable Catalysis. *Chem* **2017**, *2* (3), 313–316. https://doi.org/10.1016/j.chempr.2017.02.014.

(59) Chen, A.; Ostrom, C. Palladium-Based Nanomaterials: Synthesis and Electrochemical Applications. *Chem. Rev.* **2015**, *115* (21), 11999–12044. https://doi.org/10.1021/acs.chemrev.5b00324.

(60) Taher, A.; Nandi, D.; Choudhary, M.; Mallick, K. Suzuki Coupling Reaction in the Presence of Polymer Immobilized Palladium Nanoparticles: A Heterogeneous Catalytic Pathway. *New J. Chem.* **2015**, *39* (7), 5589–5596. https://doi.org/10.1039/c5nj00969c.

(61) Souza, F. D.; Fiedler, H.; Nome, F. Zwitterionic Surfactant Stabilized Palladium Nanoparticles as Catalysts in Aromatic Nitro Compound Reductions. *J. Braz. Chem. Soc.* **2016**, *27* (2), 372–381. https://doi.org/10.5935/0103-5053.20150284.

(62) Dhillon, S.; Kant, R. Theory for Electrochemical Impedance Spectroscopy of Heterogeneous Electrode with Distributed Capacitance and Charge Transfer Resistance. *J. Chem. Sci.* **2017**, *129* (8), 1277–1292. https://doi.org/10.1007/s12039-017-1335-x.

(63) Intruments, G. Basics of Electrochemical Impedance Spectroscopy.

(64) Jin, M.; Zhang, H.; Xie, Z.; Xia, Y. Palladium Concave Nanocubes with High-Index Facets and Their Enhanced Catalytic Properties. *Angew. Chemie - Int. Ed.* **2011**, *50* (34), 7850–7854. https://doi.org/10.1002/anie.201103002.

(65) Zhang, P.; Sui, Y.; Xiao, G.; Wang, Y.; Wang, C.; Liu, B.; Zou, G.; Zou, B. Facile Fabrication of Faceted Copper Nanocrystals with High Catalytic Activity for P-Nitrophenol Reduction. *J. Mater. Chem. A* **2013**, *1* (5), 1632–1638. https://doi.org/10.1039/c2ta00350c.

(66) Mattson, B.; Jarman, S. Estimating the amazing surface areas of the incredibly tiny https://uwaterloo.ca/chem13-news-magazine/february-2018/feature/part-2-estimating-amazing-surface-areas-incredibly-tiny.

(67) Ethylene Glycol Heat-Transfer Fluid Freezing point , viscosity , specific gravity and specific heat capacity of ethylene glycol based heat-transfer fluids , or brines Ethylene Glycol Heat-Transfer Fluid https://www.engineeringtoolbox.com/ethylene-glycol-d_146.html.

(68) Sun, T.; Teja, A. S. Density, Viscosity, and Thermal Conductivity of Aqueous Ethylene, Diethylene, and Triethylene Glycol Mixtures between 290 K and 450 K. *J. Chem. Eng. Data* **2003**, *48* (1), 198–202. https://doi.org/10.1021/je025610o.

(69) Travers, F.; Douzou, P. Dielectric Constant of Mixed Solvents Used for a Low

Temperature Biochemistry. *Biochimie* **1974**, *56* (4), 509–514. https://doi.org/10.1016/S0300-9084(74)80066-0.

(70) Maribo-Mogensen, B.; Kontogeorgis, G. M.; Thomsen, K. Modeling of Dielectric Properties of Complex Fluids with an Equation of State. *J. Phys. Chem. B* **2013**, *117* (12), 3389–3397. https://doi.org/10.1021/jp310572q.

(71) Hansen Solubility Parameters https://www.hansen-solubility.com/HSP-science/solvent-blends.php.

(72) Safo, I. A.; Werheid, M.; Dosche, C.; Oezaslan, M. The Role of Polyvinylpyrrolidone (PVP) as a Capping and Structure-Directing Agent in the Formation of Pt Nanocubes. *Nanoscale Adv.* **2019**, *1* (8), 3095–3106. https://doi.org/10.1039/c9na00186g.

(73) Slavík, P.; Kurka, D. W.; Smith, D. K. Palladium-Scavenging Self-Assembled Hybrid Hydrogels-Reusable Highly-Active Green Catalysts for Suzuki-Miyaura Cross-Coupling Reactions. *Chem. Sci.* **2018**, *9* (46), 8673–8681. https://doi.org/10.1039/c8sc04561e.

(74) Fu, Q.; Meng, Y.; Fang, Z.; Hu, Q.; Xu, L.; Gao, W.; Huang, X.; Xue, Q.; Sun, Y. P.; Lu, F. Boron Nitride Nanosheet-Anchored Pd-Fe Core-Shell Nanoparticles as Highly Efficient Catalysts for Suzuki-Miyaura Coupling Reactions. *ACS Appl. Mater. Interfaces* **2017**, *9* (3), 2469–2476. https://doi.org/10.1021/acsami.6b13570.

(75) Chatterjee, S.; Bhattacharya, S. K. Size-Dependent Catalytic Activity and Fate of Palladium Nanoparticles in Suzuki-Miyaura Coupling Reactions. *ACS Omega* **2018**, *3* (10), 12905–12913. https://doi.org/10.1021/acsomega.8b01598.

(76) Perez-Lorenzo, M. Palladium Nanoparticles as Efficient Catalysts for Suzuki Cross-Coupling Reactions. *J. Phys. Chem. Lett.* **2012**, No. 3, 167–174. https://doi.org/dx.doi.org/10.1021/jz2013984.

(77) Sun, J.; Fu, Y.; He, G.; Sun, X.; Wang, X. Catalytic Hydrogenation of Nitrophenols and Nitrotoluenes over a Palladium/Graphene Nanocomposite. *Catal. Sci. Technol.* **2014**, *4* (6), 1742–1748. https://doi.org/10.1039/c4cy00048j.

(78) Johnson, J. A.; Makis, J. J.; Marvin, K. A.; Rodenbusch, S. E.; Stevenson, K. J. Size-Dependent Hydrogenation of p-Nitrophenol with Pd Nanoparticles Synthesized with

Poly(Amido)Amine Dendrimer Templates. *J. Phys. Chem. C* **2013**, *117* (44), 22644–22651. https://doi.org/10.1021/jp4041474.

(79) Menumerov, E.; Hughes, R. A.; Neretina, S. Catalytic Reduction of 4-Nitrophenol: A Quantitative Assessment of the Role of Dissolved Oxygen in Determining the Induction Time. *Nano Lett.* **2016**, *16* (12), 7791–7797. https://doi.org/10.1021/acs.nanolett.6b03991.

(80) Narkhede, N.; Uttam, B.; Rao, C. P. Calixarene-Assisted Pd Nanoparticles in Organic Transformations: Synthesis, Characterization, and Catalytic Applications in Water for C-C Coupling and for the Reduction of Nitroaromatics and Organic Dyes. *ACS Omega* **2019**, *4* (3), 4908–4917. https://doi.org/10.1021/acsomega.9b00095.

(81) Begum, R.; Naseem, K.; Ahmed, E.; Sharif, A.; Farooqi, Z. H. Simultaneous Catalytic Reduction of Nitroarenes Using Silver Nanoparticles Fabricated in Poly(N-Isopropylacrylamide-Acrylic Acid-Acrylamide) Microgels. *Colloids Surfaces A Physicochem. Eng. Asp.* **2016**, *511*, 17–26. https://doi.org/10.1016/j.colsurfa.2016.09.076.

(82) Sreeju., N.; Rufus, A.; Philip, D. Microwave-Assisted Rapid Synthesis of Copper Nanoparticles with Exceptional Stability and Their Multifaceted Applications. *J. Mol. Liq.* **2016**, *221*, 1008–1021. https://doi.org/10.1016/j.molliq.2016.06.080.